MINISTRY OF EDUCATION AND SCIENCE OF UKRAINE
National aerospace university
«Kharkiv Aviation Institute»

Y. Martseniuk, F. Sirenko

STRENGTH ANALYSIS OF BLADE ROOT

Manual

Kharkiv «KhAi» 2016

UDC 621.452.3-226.01 (075.8)
BBL 39.15я73
M35

Описано конструкції різних способів з'єднання робочих лопаток авіаційних ГТД з дисками. Розглянуто переваги й недоліки найбільш поширених типів з'єднань. Викладено методику і наведено приклади розрахунків замкових з'єднань на міцність.

Для студентів, які вивчають курси «Конструкція і робочі процеси авіаційних двигунів і енергетичних установок», «Динаміка і міцність авіаційних двигунів і енергетичних установок», «Конструкція і міцність авіаційних двигунів», «Конструкція і міцність газотурбінних двигунів і енергетичних установок», а також при курсовому і дипломному проектуванні.

Reviewers: Doctor of Engineering Science, Associate Prof. V. Lohinov,
Candidate of Engineering Science, Associate Prof. A. Lytvyak

Martseniuk, Y.

M35 Strength analysis of blade root [Text] : manual / Y. Martseniuk, F. Sirenko. – Kharkiv: National aerospace university «Kharkiv aviation institute», 2016. – 52 p.
ISBN 978-966-662-469-0

The tutorial addresses different constructive methods to secure impeller blades to the disks of GTE, advantages and disadvantages of the most used joints, methods of the root strength analysis. Manual also comprises examples of strength analyses.

The manual is profitable for students studying “Design and Operation Processes of Engines and Power Plants”, “Dynamics and Strength of Aircraft Engines and Power Plants”, “Design and strength of Aeroengines”, “Design and Strength of gas turbine engines and power plants” and working on their diploma works.

Il. 25. Tables 7. Ref.: 10 items.

UDC 621.452.3-226.01 (075.8)
BBL 39.15я73

ISBN 978-966-662-469-0

INTRODUCTION

The strength and the reliability of the gas turbine engine (GTE) parts are posed at the design stage, and then ensured at finishing and certification.

The strength of GTE parts at the design stage is provided by the design-experimental analysis. The analysis is based on the mathematical and physical modeling of object`s behavior, models of its thermal and stress-strain state, and experience in design, development and maintenance of the prototype engine.

The methods used at design stage to ensure the strength of GTE parts are analytical. Besides, designers address the scientific and technical potential and the earned experience in engine designing and maintenance.

As a rule, the methods of strength verification at development and certification stage, as well as methods to ensure safe maintenance are experimental.

The experience in development and maintenance of aircraft GTE shows that the strength of the engine parts must be assured at design, development and certification stages. Several requirements to the strength calculations, materials and manufacturing techniques, design of parts and assemblies must be met.

Group of parts (main parts) is allocated for each new engine. Designing, development, certification and operation of these parts cause increased attention, as well as tough regulation requirements to their strength, lifetime and materials these parts are made of.

1. REQUIREMENTS TO JOINTS

Blade designing requires the simultaneous solution of all multi-aspect tasks of blade quality provision. To solve the mentioned tasks design bureau draws in the engineers from different scientific departments. Design method is based on the interactive approach. The first step of the method is getting the geometrical profile of the blade at each design section, the second – designing the blade airfoil basing on the sections obtained at the first step. Next, aerodynamic and strength performances of blade must be analyzed once again to make them more accurate. After airfoil, designers get down to blade root, tip and other elements of blade. The validation of design results is made by modern analytical and experimental methods.

The type of blade root to be used for blade securing to the disk depends on specific operational conditions of engine component.

The joints must meet common requirements set to gas turbine engines and some unique requirements set to blade roots only. The unique requirements are:

– attachment of the needed number of blades to the disk;

– provision of needed strength level of blade root at its minimum mass;

– ensuring the rigidity of each blade as identical as possible to get the self-oscillations being within the range specified by the designer;

– accurate fitting of blades to the disk and securing their position during operation;

– blades must be easy to produce, assemble and replace in maintenance.

Each root cannot entirely meet the above mentioned requirements, because lots of them are contradictory. The design of particular blade root must meet the requirements made to particular gas turbine engine.

Disk contains longitudinal slots that are usually oriented at an angle to generatrix of disk rim. Such positioning allows fitting a bigger number of blades to the disk rim. The angle of the slot must be coordinated with the blade angle at the root.

The roots and slots in the disk are broached, milled or turned.

2. TYPES OF BLADE ROOTS

2.1. Cylindrical root

Cylindrical root (Fig. 1) was widely spread in the earliest gas turbine engines (RD-20 etc.). It was simple, strong enough and light, manufacturable.

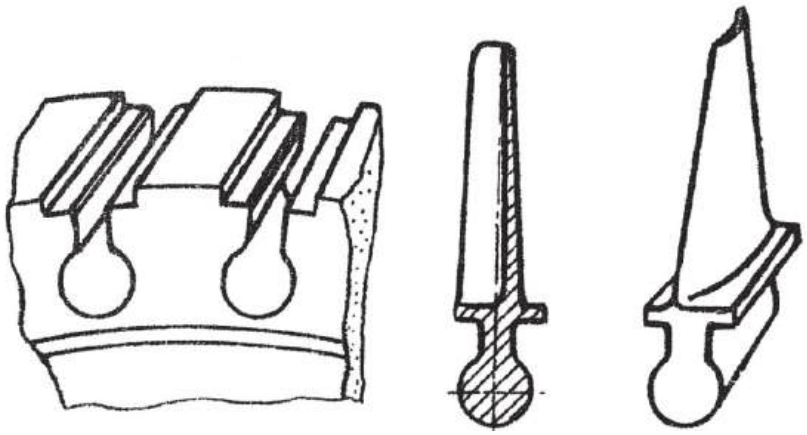

Fig. 1. Cylindrical root: a – disk rim; b – blade

This root type had a very important disadvantage. The shape of slot resulted in considerable reduction of safety margins at disk rim. This disadvantage made attachment of the needed number of blades to be a very complex problem. Staggered positioning of slots (alternation of blade roots with long and short legs) was the solution of the problem, but in its turn resulted in growth of disk rim width. Due to the above mentioned, this root is not used in modern GTE.

2.2. Dovetail root

Dovetail root has simple structure and is easy to manufacture. These features differ this root among other roots. Big contact area of blade root and slot in the disk provides good heat withdrawal from the blade.

Dovetail joint is standard to attach compressor blades to the disk for the majority of modern GTE. The blade root and the slot in the disk, being crossed by the plane perpendicular to slot axis, have trapezoidal profile (Fig. 2, a). The apex angle α of the trapezoidal profile (Fig. 2, b) equals to 30…40°. Contact surfaces of the root may be flat (Fig. 3, a) or circular (Fig. 3, b). Sometimes the curvilinear slot is used to fit the fan blades (Fig. 3, c) to the disk. This is especially widespread for the high bypass turbofans. This allows increasing the total contact area, and reducing the stresses in the lock.

Loose fit is the most common to fit blades to the disk. The clearance is 0.01…0.04 mm, so blades can be easily attached and removed. The loose fit allows miniature circumferential displacements, hence friction between contact

surfaces of dovetail joint damp the oscillations. This effect takes place, when rotational speed is less than $(0.7)n_{max}$. When rotational speed becomes higher, the centrifugal force presses the blade to the disk making the joint rigid (constrains from any displacements).

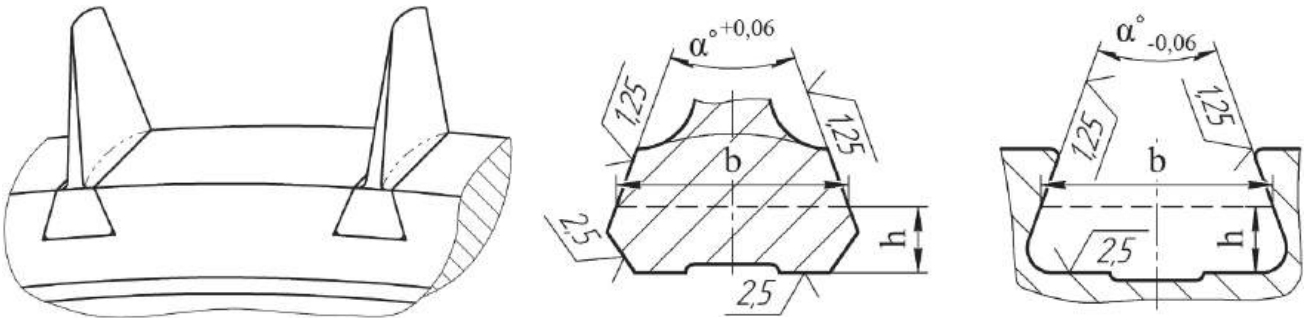

a b

Fig. 2. Dovetail joint of blades and disk:
a – assembly; b – blade root and slot in the disk

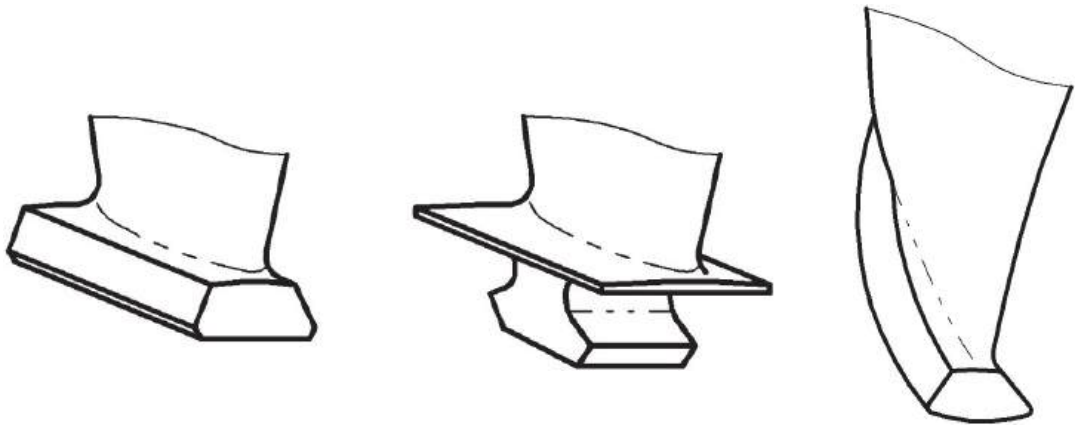

a b c

Fig. 3. Contact surfaces of root: a – flat; b – circular; c – curvilinear

When frequency of self-oscillations must be increased to move outside the operational range, then blades are fitted with negative clearance. The maximum negative clearance of the joint may reach 0.015 mm. The value of negative clearance is limited by strength considerations.

The faces of root are covered with copper or silver of 0.003…0.005 mm depth. The cover facilitates assembling and disassembling, serves as additional damping element and prevents from guide scratches that may appear at the surfaces of the root.

Regardless fitting, the blade must be constrained from displacements along the slot that may appear due to aerodynamic, centrifugal and arbitrary forces. Blade fixation can be done in different ways:

- individual fixing plates;
- axial and radial pins;
- continuous or split ring.

Individual fixing plates. Special profile dips are machined in the floor of the slot or in the root of the blade *3*. The shaped section of the plate *2* is placed in the dips (Fig. 4, a, b). After blade was fitted to the disk *1*, sides of plate are turned up or down. The plate may not have the shaped section. Flat plate has cuts or spreadings from both sides (Fig. 4, c, d). The flat plates constrain blade from displacements along the slot by turning side elements both up and down.

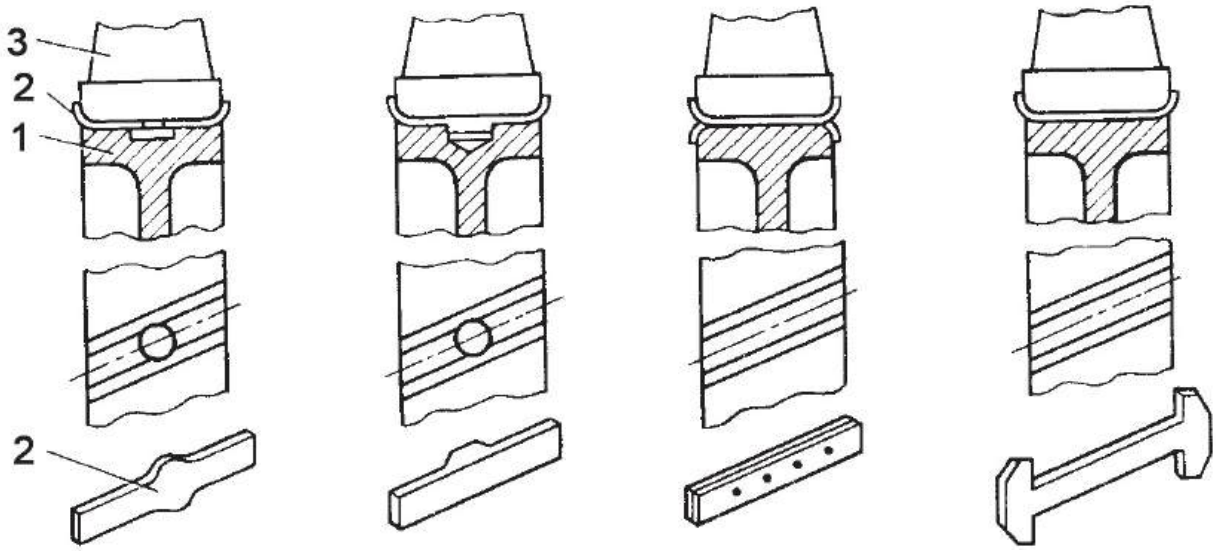

Fig. 4. Blade fixation by individual plates

Blade can be fixed by the plate *2* on one side and by press-fitted pin *4* on the other side (Fig. 5, a).

Axial pins. Orifices for roll pin or grub screw *5* are drilled after impeller has been assembled. The orifices are placed at the contact between blade root *3′* of impeller blade *3* and floor of the slot (Fig. 5, b). The downstream impeller stage prevents pins from dropping out from orifices. This fixture is non-repairable and turns to stress concentrators (grub screw only), which in their turn result in lower fatigue strength of disk and blade. These are main shortcomings of this fixation method.

Radial pins. Orifices for radial pins (Fig. 5, c) are drilled in the disk *1* and the blades *5* separately. Next, safety sleeve *6* is mounted in each orifice. After impeller has been assembled, the orifices in the blades and the disk are matched. The blade is pinned to the disk and prevented from pin *4* dropping out from orifice by turning in the feather of safety sleeve.

Continuous ring. The ring *2* is fitted with the transition fit in the annular slot, turned in the disk *1*. The root component of the blade has slots that constrain

blade displacement along the slot of the disk (see Fig. 5). Ring turning is constrained by radial pin.

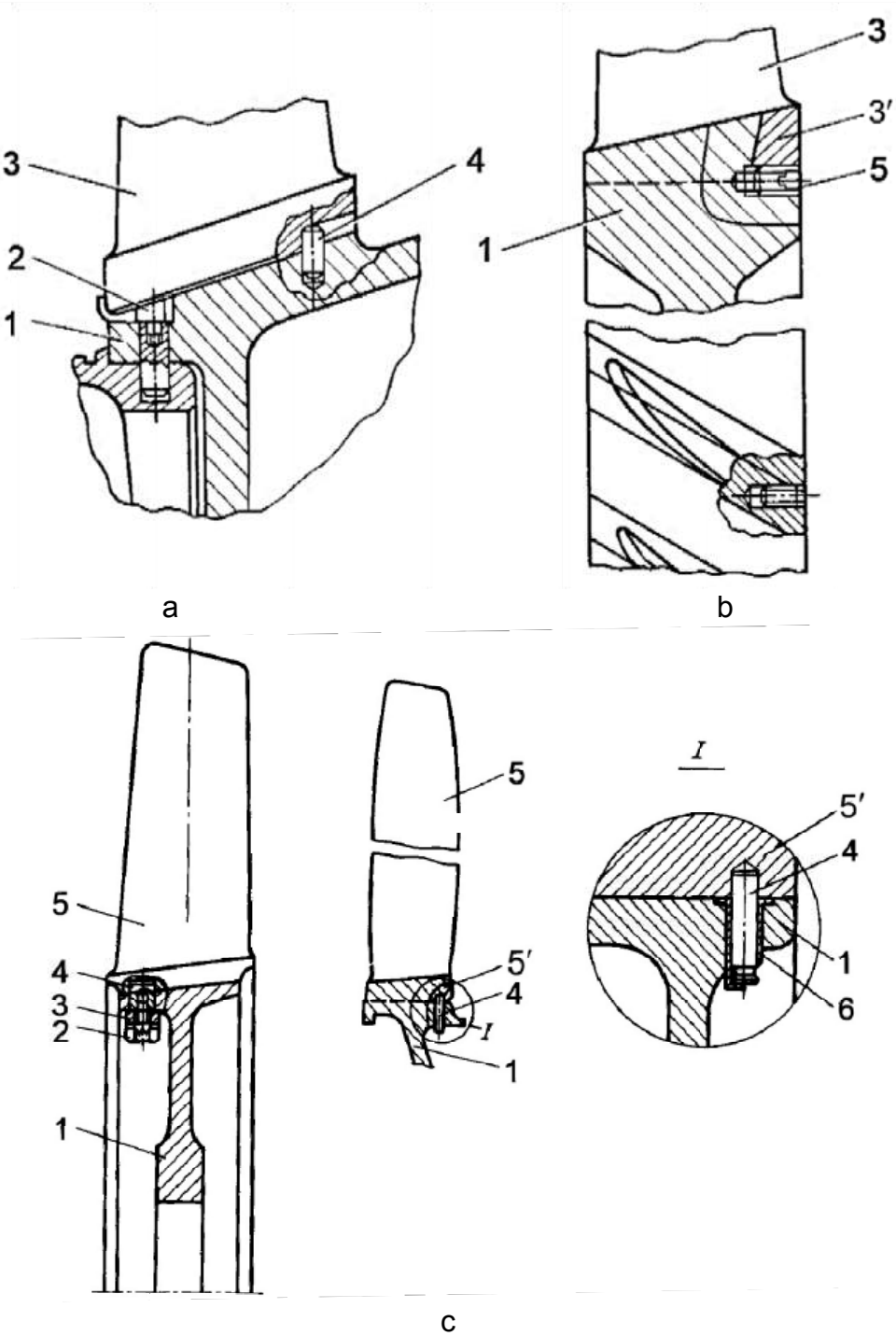

Fig. 5. Impeller blade fastening by continuous ring and pins

Split rings. The C-ring *1* is fitted in the slot *6*, which is turned in the disk *4* and blades *2* (Fig. 6). The ring is common for the disk and the blades. The ring is pressed to blades under centrifugal force action during operation. It is constrained from circumferential displacements by the stop *3*. Fixation is needed to prevent gap of ring mate the blade root. There are special orifices *5* in the disk to dismount

ring while blade replacement. Common C-ring improves the mutual positioning of blades (all blades are at one plane) and hence, the stability of balancing.

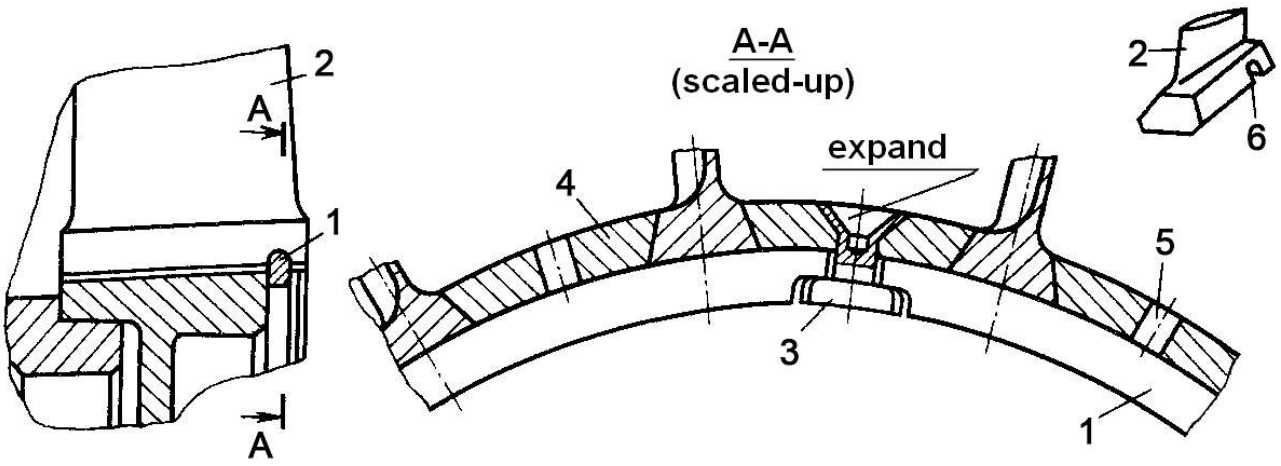

Fig. 6. Impeller blade fixation by common C-ring

2.3. Impeller blade fixation in an annular slot

Fixation of blades (see Fig. 3, b) in annular slot (Fig. 7) is manufacturable in assembling, allows attachment of needed number of blades of each stage and weakens to a lesser extent the drum component of the rotor than the dovetail joint.

Blades 2 jointly with safety lock 3 are mounted in annular slot 4 one by one through the port 5. Next, the whole set of blades is displaced on the half of blade pitch. The port becomes closed. The set is constrained from circumferential displacements by grub screws. There are tow special adjacent blades, which have special slots 6 to fit the lock.

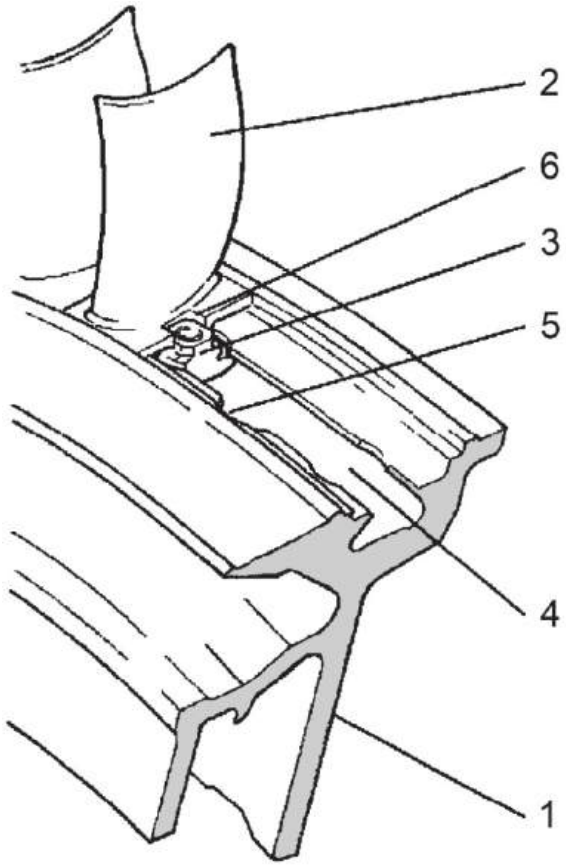

Fig. 7. Impeller blade mounting in annular slot:
1 – disk; 2 – blade; 3 – safety lock;
4 – annular slot; 5 – port to insert the blades and the lock in the annular ring;
6 – slot in the blade for lock fixation purposes

2.4. Pinned root

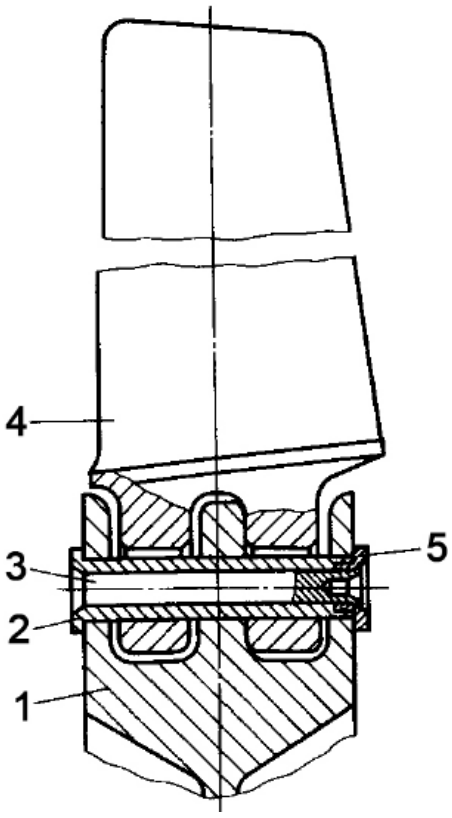

Fig. 8. The scheme of pinned root

The anatomy of the root requires the blade *4* to be fitted with positive clearance relative to pin *2* and disk *1* (Fig. 8). Pin is constrained from displacements by shoulder-head bushing *5* and rivet *3* that is flared in the bushing. Loose fit allows blade turning round the pin under centrifugal and gas dynamic forces. The pin is press-fitted to the disk. The bending moments of centrifugal and gas dynamic forces are virtually mutually compensated. Hence, bending stresses in the blade become minimal and are usually neglected in the strength analysis.

Pinned joint eliminates resonant oscillations of low vibration modes and two or three times reduces vibration stresses at the rest vibration modes in comparison to dovetail root. Stress reduction happens due to sliding friction in the hinge and aerodynamic damping. But the mobility of the joint may tend to increase wear or fretting[1] of blades, disk and pins. Special arrangements must be made to fail-safe the joint, for example, cover joint surfaces (face and ends of orifice in the blade root, outer surface of pin) with solid lubricant on basis of molybdenum disulfide. The other method to protect wear surfaces of the joint is coating them with wear-resistant coating.

Blade tips of the assembled impeller cannot be machined, which is needed for minimum radial clearance. Moreover, blades with pinned root are the heaviest ones compared to other blades. The above mentioned disadvantages limit the application range of blades with pinned root part. They are used for impellers that operate at relatively low circumferential speed of blade tip (less than 320 m/s). For other blades it is impossible to provide the strength of disk rim and pin itself. This root is for the most part applied for low pressure compressor of turbojets and turbofans with low bypass ratio. The pinned root is not spread in modern engines.

2.5. Fir-tree root

The scheme of fir-tree joint is presented in Fig. 9.

[1] Fretting refers to wear of material in hostile environment, which appears on contacting surfaces due to relative motion of parts.

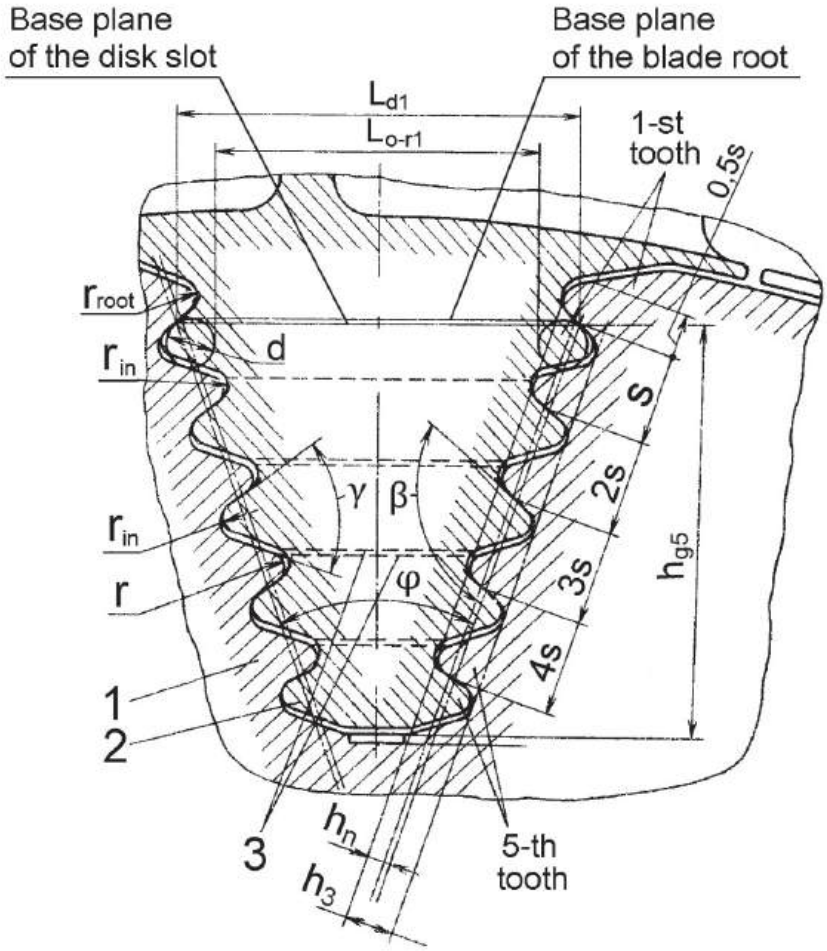

Fig. 9. Fir-tree joint

The over-rolls dimension $L_{o\text{-}r}$ of corresponding neck of the slot can be increased for integer value (reference values are presented in tables). The rest $L_{o\text{-}r}$ dependent values are also accordingly increased. This is important for cooled blades.

Main dimensions of blade root and slot to fit the blade, number of tooth pairs are described in design documentation (Table 1).

Table 1. Recommended main parameters of fir-tree root

S, mm	***φ*°**	***γ*°**	***β*°**	Number of tooth pairs ***q***
		Extreme deviation		
		±30'	±15'	
1.8; 2.0; 2.2; 2.4; 2.6; 2.8; 3.0; 3.2; 3.5	20	65	115	2
1.8; 2.0; 2.2; 2.4; 2.6; 2.8; 3.0; 3.2; 3.5; 4.0; 4.5; 5.2; 6.0	30	55	105	2…5
		65	115	
	40	55	105	
	50			

All teeth of the joint must operate at similar conditions. This avoids dangerous local overloads of joint components. To provide similar operational conditions, all contact surfaces must be evenly adjoined as along the contact length b_i (see Fig. 16), so along the contact width (see Fig. 17, a). Hence, contact surfaces of root and disk rim must be manufactured at increased accuracy.

Fir-tree root found its wide use in gas turbines due to the following advantages:

1. Wedge shape of blade root and disk rim component provides almost uniform stress distribution (rim width and impeller mass are minimum).
2. Relatively small dimensions of the slot and wedge component of the blade root allow placing big number of blades. Sometimes, twin roots are applied to fit more blades to the disk.
3. Clearance fit of the blade in the slot prevents thermal stresses in the joint.
4. The clearance between non-contact surfaces of the root and the disk rim can be used as the channels to deliver secondary air to the root component of the blade for cooling purposes.
5. Blades can be easily replaced, while overhaul or in case of their damage.

The root has the set of disadvantages along with the advantages.

1. Stresses concentrate nearby necks with small neck radius.
2. The slots in the disk and blade roots must be manufactured at high accuracy. The increased requirements are made for pitch s, angles φ, γ, β and other parameters of teeth to make the loading more even. So, deviation for the pitch is 0.008…0.016 mm, for radiuses of neck r_n and teeth r – 0.05 mm. The tolerance of slot (root) machining is checked by given over-rolls dimensions $L_{o\text{-}r}{}^{+(0.02\ldots0.05)}$. To measure over-rolls dimension the inspector places d-diameter rollers in the corresponding necks (see Fig. 9).

On the one hand, the higher number of tooth pairs is, the lower loading is taken by each pair, but on the other hand, the higher number of tooth pairs is, the more intense stress concentration is due to smaller neck radiuses of root r_n. That is why small number of tooth pairs is a preferential design.

The shape of grade from the shroud to the top tooth influences the stresses in the root. To reduce the stress concentration in the shroud neck (top one neck), the shroud neck radius r_{sh} is chosen twice bigger than other neck radiuses r_n.

The clearance between contact surfaces of blade root and slot makes up 0.2…0.3 mm that makes blade tip oscillate in circumferential direction $\delta = \Delta \frac{l}{qS}$, where l is entire length of blade (airfoil and root parts), q is a number of tooth pairs, S is a tooth pitch. When rotational speed of rotor breaks the $(0.5\ldots0.7)\omega_{max}$ margin the blade becomes jammed in the slot. It is obvious that blades in blade

kit are not similar because of deviations, which are limited by manufacturing tolerance. It was experimentally proved that jamming in the upper part of the root tends to increase in vibration stresses, and inversely, if jamming happens in lower part then vibration stresses are reduced. The difference in vibration stresses is determined by damping blade oscillations. Therefore, it is reasonable to design blade root with pitch of bottom tooth pairs being lower than pitch of upper ones.

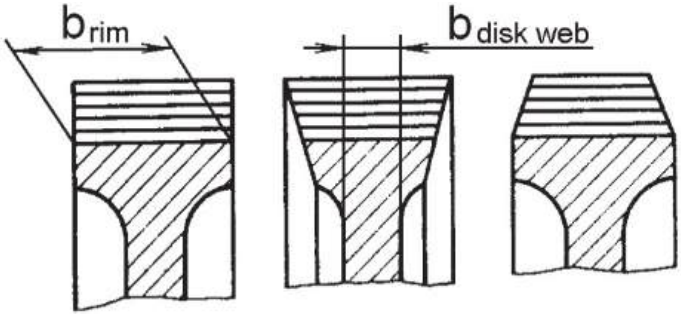

Fig. 10. The shape of disk rim with fir-tree slots

The width of rim component b_{rim} is designed to be bigger than width of disk web $b_{disk\ web}$ (Fig. 10), which reduces the stresses in the joint. The most loaded section of disk rim is the most bottom pair of minimum distant surface section. The most loaded section of blade root component is the uppermost pair of minimum distant surface section. The disk rim can be:

– constant width for disk with high blade chord to pitch ratio (Fig. 10, a);

– narrowing down width for disks with moderate blade chord to pitch ratio (Fig. 10, b), which makes disks thinner with lighter rim component;

– narrowing up width (Fig. 10, c), which reduces a contour distributed load acting the disk.

Similar to the dovetail root blades, fir-tree root blades are constrained from displacements along the slot by different design fasteners. The most used fasteners are:

1. Fixation by adjacent rotor components, e.g. rim component of the cover disks, adjacent disks, labyrinth seals (Fig. 11, a). Each one part constrains blade from one-way displacement. Fixation is not the only function of the fasteners. They also may serve to prevent gas flow being in contact with the blade root, form cavities for cooling air delivery, improve the efficiency of blade root cooling;

2. Fixation by special plates and C-rings (Fig. 11, b), which prevents blade from displacements in two opposite ways. At the same time they seal the joint and prevent air bleeding through clearances between root and disk lobes;

3. Individual fixing plates – two-side (Fig. 11, c, d) and one-side.

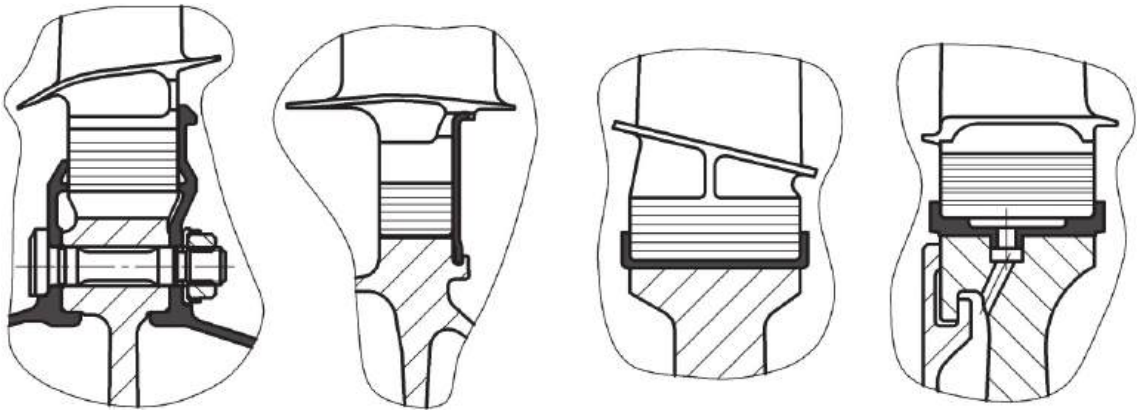

Fig. 11. Constrains of fir-tree blades from displacements along the slot

Fir-tree roots are basic for turbine blade securing to the disk. Blades of fan may have fir-tree roots with two tooth pairs. This is actual, while it is a problem to place a big number of bulky fan blades.

3. BLADE JOINT ANALYSIS ASSUMPTIONS

Blade joint transfers all loads affecting impeller blade to disk. It also loads the disk with centrifugal force of its own mass. Different temperature and linear expansion coefficient of blades and disk and uneven temperature distribution along disk radius result in great thermal loads origination. The loads result in circumferential compression stress. The lion`s portion of total load takes centrifugal force, which may reach 100…250 kN. The vast majority of existing aircraft GTE have turbine blades with the following distribution of stress at hub section: 60-70% of total stress takes centrifugal force initiated by the mass of blade airfoils, 30-40% – the rest forces. The strength of joints becomes lower at high temperature operation, which is especially actual for turbine components. The physical properties of materials turbine blades and disks are made of depend on temperature.

The strength analysis of joint consists of root analysis and rim component of disk (slotted part) analysis.

In case joint comprises fasteners (e.g. pins or studs), they also must be analyzed to check they meet strength requirements.

The method of simplified analysis allows comparative estimation of root strength. Mode of maximum rotational speed at maximum ambient temperature is adopted to be the design mode for the analysis.

Generally, true stress is one and a half or two times higher than stress obtained from the strength analysis. The mentioned fact is considered upon safety factor calculation. The limiting stress is taken understated.

The safe stresses for each root component type are set by virtue of statistics of existing roots that had successfully fulfilled the specified lifetime of gas turbine engines.

Simplified analysis usually considers blade to be loaded by centrifugal forces of blade (airfoil and root components). Loads that appear due to gas flow are usually neglected.

Hence, the method of simplified blade root strength analysis is based on the following assumptions:

1. blade root is exposed to centrifugal force only;

2. centrifugal forces of airfoil $\boldsymbol{P_{centr\ airfoil}}$ and root $\boldsymbol{P_{centr\ root}}$ act in the same plane, which passes through the gravity center of root;

3. centrifugal force of the airfoil and the root is distributed between contact surfaces of root proportionally to their areas.

Considering assumptions made for these analyses and airworthiness standards, the safety factor for elements of the joint must be equal to $\boldsymbol{[k] = 3}$.

4. STRENGTH ANALYSIS OF BLADE JOINT

4.1. Method of dovetail root analysis

Let`s consider the most general case, when gas path of compressor is of constant external radius. Then, slots to mount the blades to the disk are tilted relatively axis of rotation. The design scheme of the joint is shown in Fig. 12. According to the scheme, elements of joint are exposed to centrifugal force of airfoil and root and centrifugal force of steeple.

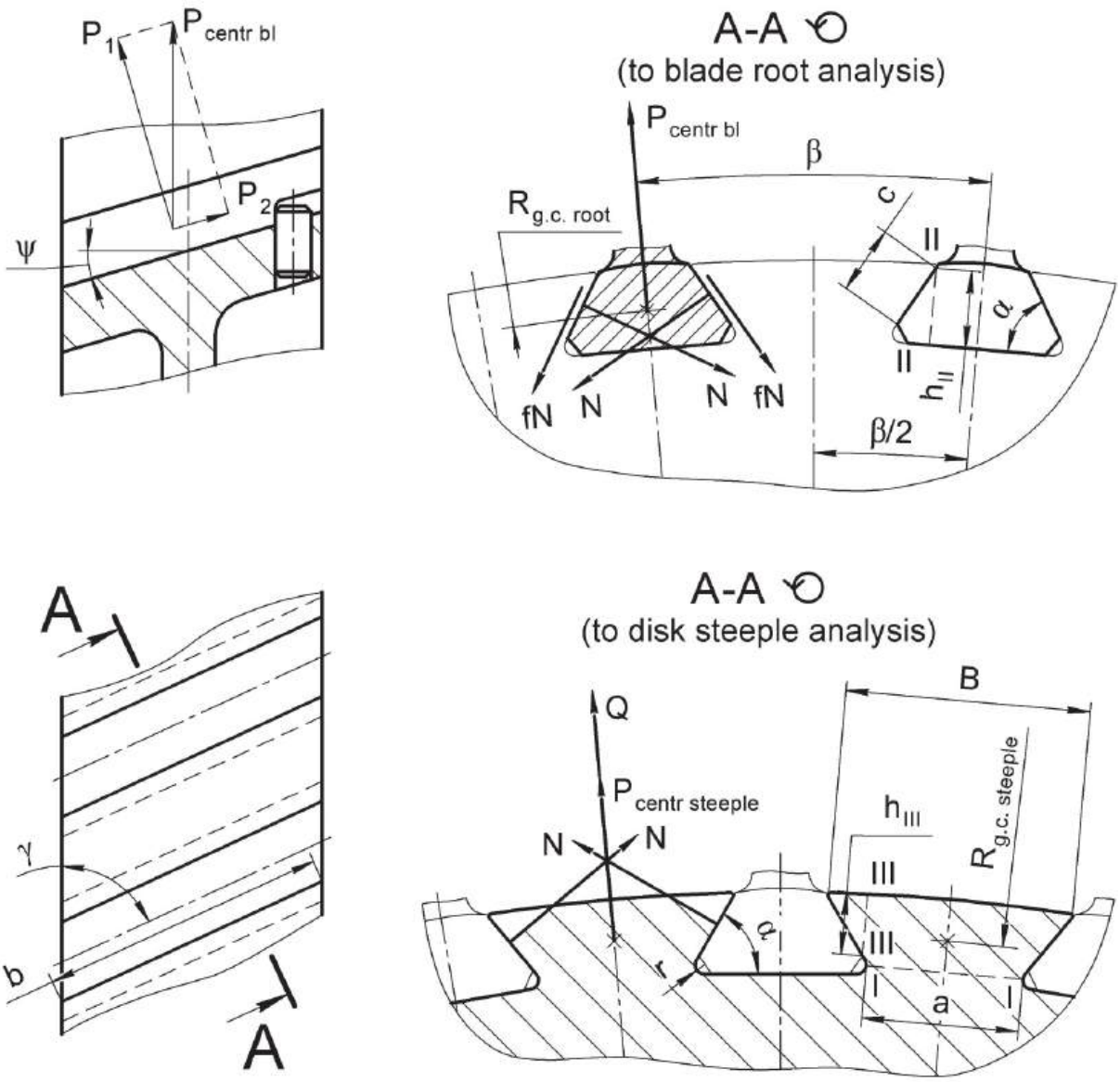

Fig. 12. The design scheme of dovetail root analysis

Here is the list of stress to be determined in the analysis of dovetail root:

– tensile stress at the neck of the steeple σ_t (section I–I) generated by the centrifugal forces of blade and steeple;

– bearing stress σ_{bear} at contact surfaces of blade root;

– shearing stress at the section II–II ($\tau_{shear\ II}$) of blade root and section III–III ($\tau_{shear\ III}$) of steeple generated by the centrifugal force of the blade.

The impeller blade consists of the airfoil 1 and the root 3 (Fig. 13). The blade body must be conjugated with the root in the way to escape stress concentration. Blade with high aspect ratio may have shroud plate (turbine blade is normally shrouded).

The centrifugal force acting the joint consists of centrifugal force of airfoil, shroud plates (inner shroud, see Fig. 3, b, and outer shroud, if available) and root (see Fig. 13):

$$P_{centr\ bl} = P_{centr\ airfoil} + P_{centr\ sh\ pl} + P_{centr\ root} = \\ = \sigma_{tens\ root} F_{airfoil\ root} + m_{sh\ pl} R_{sh\ pl} \omega^2 + \\ + m_{root} R_{g.c.\ root} \omega^2, \qquad (1)$$

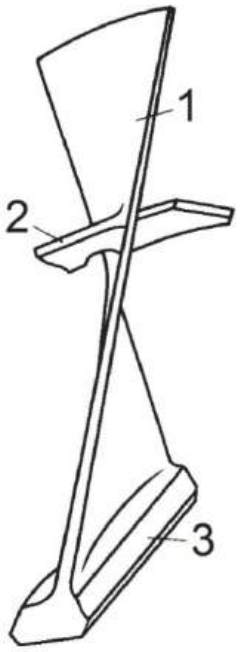

Fig. 13. Compressor blade: 1 – airfoil; 2 – shroud plate; 3 – root

where $\sigma_{tens\ root}$, $F_{airfoil\ root}$ are tensile stress at root and area of root respectively (the stress and area were obtained in blade strength analysis);

$m_{sh\ pl}$, $R_{sh\ pl}$ are mass and gravity center of shroud plate;

m_{root}, $R_{g.c.\ root}$ are mass and gravity center of root;

ω – angular velocity.

The centrifugal force of blade $P_{centr\ bl}$ can be decomposed into two forces P_1 and P_2 (see. Fig. 12). The force P_1 is balanced by reactions N at plane A-A, which is perpendicular to the slot longitudinal axis. The reaction N is directed along the normal to contact surface. Hence, the following equation can be obtained from equilibrium condition for the blade and considering friction in contact pairs:

$$P_1 = 2N\cos\alpha + 2fN\sin\alpha, \qquad (2)$$

whence

$$N = \frac{P_1}{2\cos\alpha + 2f\sin\alpha} = \frac{P_{centr\ bl}\cos\psi}{2\left(\cos\alpha + f\sin\alpha\right)}, \qquad (3)$$

where ψ – angle between slot floor and the axis of rotation;

α – flank angle (angle between contact surface and floor of slot);

f – coefficient of sliding friction, averaged value for steel is 0.15…0.18, for aluminum – 0.3, for titanium – 0.4...0.6.

The force P_2 loads fastener that prevents blade displacement along the slot. The bearing stress acting contact surfaces of root and slot must be calculated as

$$\sigma_{bear} = \frac{P_{bear}}{F_{bear}} = \frac{N}{c \cdot b}, \tag{4}$$

where ***c*** and ***b*** are length and width of contact surface.

Tensile stress at the neck of the steeple is initiated by reactions of adjacent blades N and centrifugal force of the steeple $P_{centr\ steeple}$.

$$\sigma_{tens} = \frac{P_{tens}}{F_{tens}} = \frac{Q}{a \cdot b}, \tag{5}$$

where ***a*** – neck width;

b – slot length at neck section;

Q – tearing force, which acts the steeple. It is calculated from equilibrium condition as

$$Q = 2N\cos\left(\alpha - \frac{\beta}{2}\right) + P_{centr\ steeple}. \tag{6}$$

Here $\beta = 360/z$ is the angle between the adjacent slots. The number of the slots is equal to ***z***.

True stress must consider the stress concentration, which is presented by a concentration factor a_{conc} = (1.3…3). The concentration factor depends on fillets of the slot. The higher radius of fillet, the lower stress concentration is

$$\sigma_{tens\ max} = a_{conc}\sigma_{tens}\ . \tag{7}$$

The most bladelike test specimen is a rectangular plate with the symmetrical notches (Fig. 14). The concentration factor for the test specimen is widely presented in the reference books. The minimum distance between the notches of the test specimen (size ***b*** in Fig. 14) corresponds to the neck of the steeple (size ***a*** in Fig. 12); the width of the test specimen (size ***B*** in Fig. 14) in its turn corresponds to the steeple width at the outer radius of the disk.

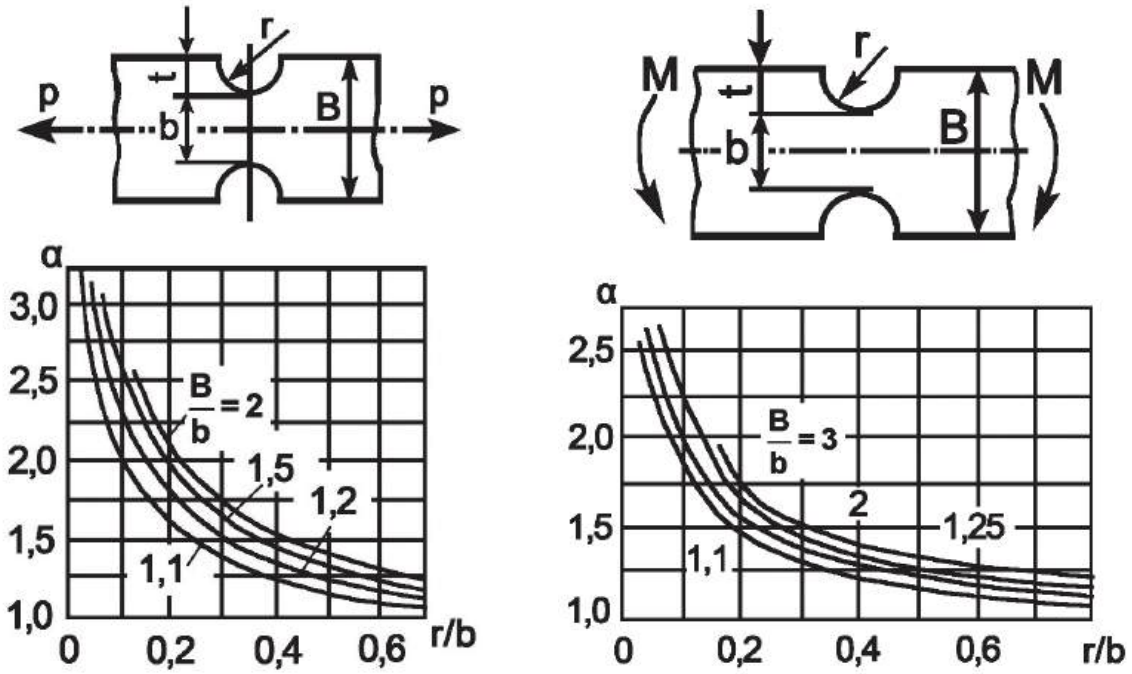

a b

Fig. 14. Diagrams of the observed concentration factor for the rectangular plate: a – tension, b – bending

Shearing stress that arises in the root component of the blade due to the centrifugal force can be calculated as

$$\tau_{shear\ II} = \frac{P_{centr\ bl}}{2F_{sh\ bl}} = \frac{P_{centr\ bl}}{2h_{II}b}\ , \tag{8}$$

where h_{II} is a width of the root at the cross-section II–II (the cross-sectional area of the material with the area parallel to the applied force vector).

The shearing stress that arises in the steeple of the disk due to the centrifugal force can be calculated as

$$\tau_{sh\ III} = \frac{P_{centr\ bl}}{2F_{sh\ disk}} = \frac{P_{centr\ bl}}{2h_{III}b}\ , \tag{9}$$

where h_{III} is a width of the steeple at the cross-section III–III.

The reaction N also generates the bend and the torsion of disk. But the generated stresses are small and they are usually neglected. Bending moments, which are generated by gas and centrifugal forces, are balanced by moments, which are generated by non-symmetrical loads acting contact surfaces. If the blade is exposed to the vibrations, then a bearing stress may provoke the contact corrosion at the work surfaces of the root. The fatigue cracks in the root and the disk rim appear in the areas of the stress concentration.

Bearing and tensile stresses in the modern roots, made of different materials, are presented in Table 2.

Table 2. Stresses in the modern dovetail roots

Material of the disk or the blade	σ_{bear}, MPa	σ_{tens}, MPa
Aluminum alloy	60…160	40…80
Steel	200…400	120…300
Titanium alloy	120…280	80…160

The adoption of resolution about joint strength is made on the base of the safety factors for each stress separately.

4.2. Method of pinned root analysis

The strength of the pinned root (see Fig. 8) depends on the strength of its elements and the platform portion. The main load acting the mentioned elements is the centrifugal force generated by airfoil and root. The design scheme of the pinned root is presented in Fig. 15.

Here is the list of stress to be determined in the analysis of the pinned root:

– tensile stresses σ_t at the weakness sections of the root and the platform portions;

– maximum contact stress;

– bearing stress σ_{bear} that arise between the pin and the platform portions;

– shearing stress τ_{shear} that arise in the platform portion and the pin.

The tensile stress σ_t at A-A section of the blade portion (Fig. 15, b) are calculated as

$$\sigma_{t\ bl} = \frac{P_{centr\ airfoil} + P_{centr_2}}{F_{eye}} = \frac{P_{centr\ airfoil} + P_{centr_2}}{(D-d)\sum_{i=1}^{k} b_i}, \qquad (10)$$

where $P_{centr\ airfoil}$ is the centrifugal force generated by the airfoil component of the blade;

P_{centr_2} is the centrifugal force of the upper part of the pinned root (the root above A-A cross-section);

F_{eye} is the A-A cross-section area of the eye;

D is the outer diameter of the eye;

b_i is the width of the i^{th} root portion;

d is the inner diameter of the eye;

k is the number of root portions.

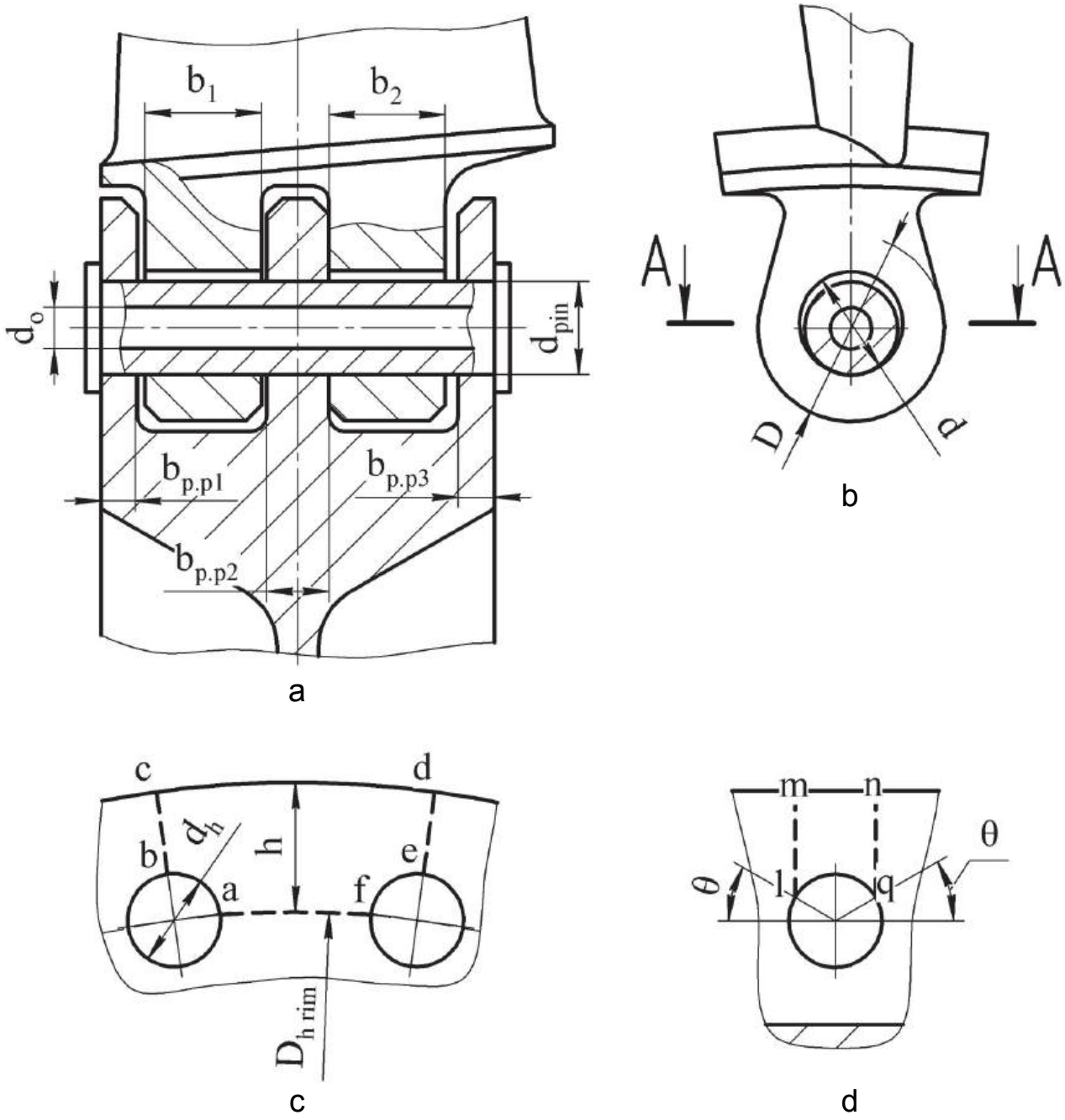

Fig. 15. The design scheme of pinned root

Maximum contact stress is calculated as (the Poisson`s ratio of materials that are in contact must be equal)

$$\sigma_{contact} = 0.798\sqrt{p\frac{d - d_{pin}}{d\ d_{pin}}\frac{E_1E_2}{\left(1-\mu^2\right)\left(E_1+E_2\right)}}\ , \qquad (11)$$

where p – contact line length distributed load,

$$p = \frac{P_{centr\ bl}}{\sum_{i=1}^{k} b_i}. \qquad (12)$$

Here $P_{centr\ bl}$ is a centrifugal force of the entire blade; E_1 and E_2 are elastic moduli of contacting materials (root portion and the pin or the pin and the platform portion); μ is the Poisson`s ratio; d_{pin} is the diameter of pin; k is the number of root portions.

Tensile stress at the weakness section of the platform portion is calculated by the following formula (the axes of holes for pins form the weakness section, see Fig. 15, c):

$$\sigma_{tens\ p.p} = \frac{P_{centr\ \Sigma}}{F_{rim}} = \frac{P_{centr\ \Sigma}}{\left(\frac{\pi}{z} D_{h\ rim} - d_h\right) \sum_{i=1}^{s} \left(b_{p.p}\right)_i}, \qquad (13)$$

where $D_{h\ rim}$ is a diameter of the circle, which is set of all hole centers in a plane that are at a given distance from the axis of rotation;

d_h is a diameter of the hole for the pin in the platform portion;

$(b_{p.p.})_i$ is a width of the i^{th} platform portion;

s is the number of platform portions ($s=k+1$);

z is the number of blades to be secured;

$P_{centr\ \Sigma}$ is a total tensile force that arises the destruction of the platform portions

$$P_{centr\ \Sigma} = P_{cent\ bl} + P_{centr\ pin} + \sum_{i=1}^{s} \left(P_{centr_4}\right)_i. \qquad (14)$$

Here $P_{centr_{pin}}$ is the centrifugal force of the pin; $\left(P_{centr_4}\right)_i$ is the centrifugal force of the sector «a-b-c-d-e-f» of the i^{th} platform portion (see Fig. 15, c).

Bearing stress that arise between the root portion and the pin

$$\sigma_{bear\ \ root\ portion} = \frac{P_{centr\ bl}}{d_{pin} \sum_{i=1}^{k} b_i}. \qquad (15)$$

Bearing stress that arise between the pin and the platform portion

$$\sigma_{bear\ platf\ portion} = \frac{P_{centr\ bl} + P_{centr\ pin}}{d_{pin} \sum_{i=1}^{s} \left(b_{platf\ portion} \right)_i}. \quad (16)$$

Shearing stress in the disk rim (Fig. 15, d)

$$\tau_{shear\ platf\ portion} = \frac{P_{shear\ \Sigma} \cos\theta}{\left(2h - d_{pin} \sin\theta \right) \sum_{i=1}^{s} \left(b_{platf\ portion} \right)_i}, \quad (17)$$

where

$$\theta = \arcsin\left(\frac{d_{pin}}{2h} \right); \quad (18)$$

h is a distance between the hole for pin fitting and outer surface of the disk;

$P_{shear\ \Sigma}$ –is a total shearing force, which is equal to

$$P_{shear\ \Sigma} = P_{centr\ bl} + P_{centr\ pin} + \sum_{i=1}^{s} \left(P_{centr_5} \right)_i \approx 1.025 \left(P_{centr\ bl} + P_{centr\ pin} \right). \quad (19)$$

Here $\left(P_{centr_5} \right)_i$ is a centrifugal force of the sector «*l-m-n-q*» of the i^{th} platform portion (see Fig. Fig. 15, d).

Shearing stress that arises in the pin is calculated as

$$\tau_{shear\ pin} = \frac{P_{centr\ bl} + P_{centr_6}}{\frac{\pi}{4} n_0 \left(d_{pin}^2 - d_{app}^2 \right)}, \quad (20)$$

where P_{centr_6} is a centrifugal force generated by the pin portion mass. The length of this portion is equal to the sum of the root portion widths $\sum_{i}^{k} b_i$;

d_{app} – the diameter of the inner aperture in the pin;
n_0 – the number of shear planes ($n_0 = 2k$).

The value of centrifugal force generated by elements, which load the joint, can be obtained from the relations

$$P_{centr\ airfoil} = \sigma_{tens\ root\ airfoil} F_{root\ airfoil}, \quad (21)$$

$$P_{centr\ j} = m_j \cdot R_{g.c\ j} \cdot \omega^2, \quad j = 2,...,6, \quad (22)$$

where $\sigma_{tens\ root\ airfoil}$ is the tensile stress at the root section of the blade;

$F_{root\ airfoil}$ is an area of the root section of the blade;

m_j – mass of the element, which loads the joint;

$R_{g.c\ j}$ is the radius of gravity center of the element, which is measured relatively to axis of rotation;

ω – angular velocity.

The stresses in the modern pinned roots, made of different materials, are presented in Table 3.

Table 3. Stresses in the modern pinned roots

Material of the disk or the blade	σ_t, MPa	$\sigma_{bear\ root\ portion}$, MPa	$\sigma_{bear\ platf\ portion}$, MPa	$\sigma_{contact}$, MPa
Steel	200	120…250	200…450	700…1800
Titanium alloy	150	100…170	180…400	650…800

4.3. Method of fir-tree root analysis

Forces, which are directed in parallel to symmetry plane of the root (Fig. 16), are balanced when

$$P_{centr\ bl} - 2\sum_{i=1}^{q} P_i = 0 \quad (23)$$

where q is the number of teeth pairs, whence the equations to calculate unknown reactions P_i can be deduced. But the set of equations is $(q-1)$ times statically indeterminate. To cope with the mentioned problem and to simplify the analysis of the fir-tree root a linear force is considered to be even for all teeth. The linear force is a ratio of force and length this force is distributed:

$$\frac{P_{centr\ bl}}{\sum_{i=1}^{n} b_i} = \frac{2P_i}{b_i}, \tag{24}$$

where b_i is the length of the contact surface of the i^{th} tooth pair.

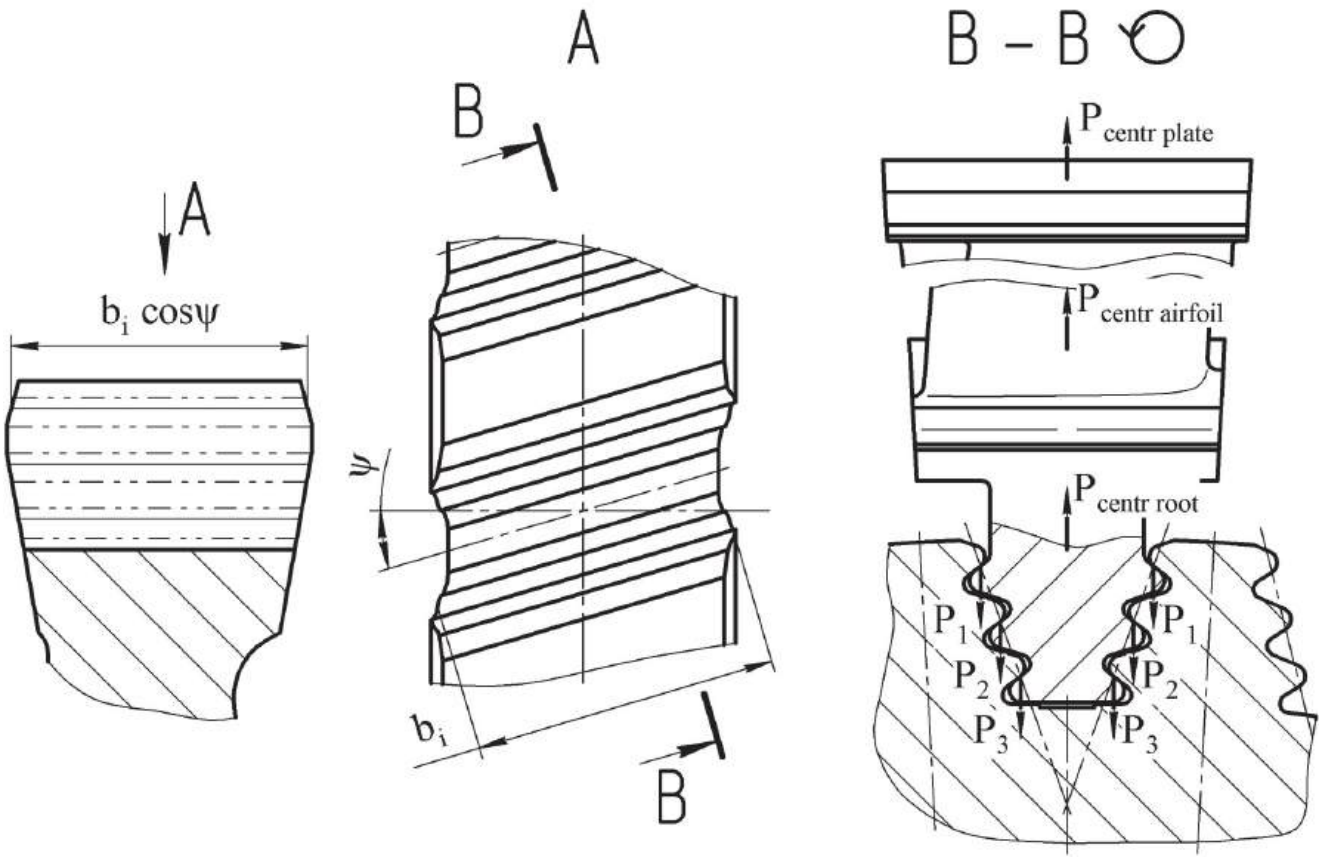

Fig. 16. Design scheme to calculate reactions that arise at contact surfaces

The assumption is made because the stresses are redistributed (averaged) in the local area. The redistribution is caused by material plasticity that originates when the root operates at high temperature. The formula (24) can be used when the width of contact surfaces is similar for all teeth.

The centrifugal force (Fig. 17, a) acting the contact surfaces generates the reaction. The reaction, which acts the i^{th} tooth of the root, is determined as

$$N_i = \frac{P_i}{\cos\theta} = \frac{P_{centr\ bl}}{2\cos\theta} \frac{b_i}{\sum_{i=1}^{q} 2b_i}, \tag{25}$$

where $\theta = \frac{\varphi}{2} + (\beta - 90°)$ is an angle between the contact surface and the symmetry plane of tooth;

β is the angle between "wedge" line and a normal to the contact surface of the tooth;

φ is the wedge angle of the tooth slot (blade root);

q is the number of tooth pairs.

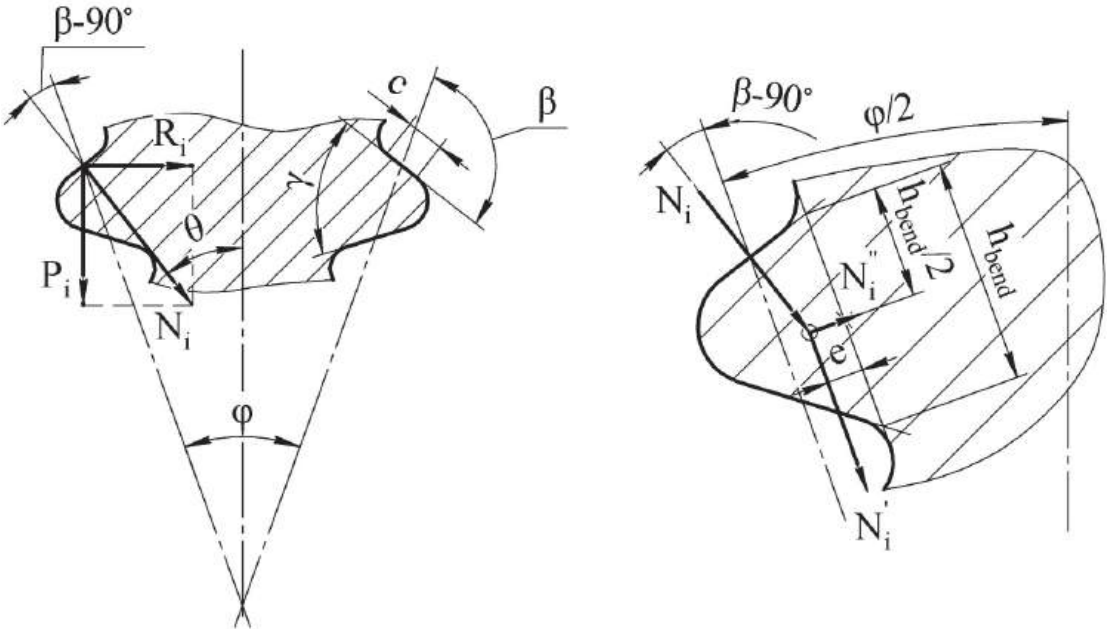

a b

Fig. 17. The design scheme of the fir-tree joint:
a – bearing strength analysis of the tooth; b – bending strength analysis of the tooth

If two blades are fitted in one slot, then the reaction acting the i^{th} tooth must be doubled.

$$N_i = \frac{P_{centr\ bl}}{2\cos\theta} \frac{b_i}{\sum_{i=1}^{q} b_i}. \quad (26)$$

The bearing stress that is generated at the contact surface of the i^{th} tooth (Fig. 17, a)

$$\sigma_{bear_i} = \frac{P_{bear_i}}{F_{bear_i}} = \frac{N_i}{cb_i}, \quad (27)$$

where c is a width of the contact area at the section perpendicular to slot. The width is similar for all teeth.

The bending stress is determined as

$$\sigma_{bend_i} = \frac{M_{bend_i}}{W_{bend_i}}. \tag{28}$$

To calculate bending moment it is necessary to determine arm of reaction that loads the tooth. The point is the intersection of the line of the reaction and a normal to a base of tooth. The normal halves the base of tooth (Fig. 17, b). A bending force will be equal to the reaction component (N_i'), which is parallel to the tooth base. Thus, the bending moment is calculated as

$$M_{bend_i} = N_i \cos(\beta - 90°) e, \tag{29}$$

where e is an arm of reaction.

The section modulus for rectangular cross-section is determined as follows

$$W_{bend_i} = \frac{b_i h_{bend}^2}{6}, \tag{30}$$

where h_{bend} is the height of tooth base (see Fig. 17, b).

Formula for bending stress originating at the base of the ith tooth is deduced considering formulas (29) and (30)

$$\sigma_{bend_i} = \frac{6 N_i \; e \cos(\beta - 90°)}{b_i \cdot h_{bend}^2}. \tag{31}$$

Maximal shearing stress is generated by the reaction component, which is parallel to the tooth base (Fig. 18, a):

$$\tau_{shear} = \frac{P_{shear}}{F_{shear}} = \frac{N_i \cdot \cos(\beta - 90°)}{b_i \cdot h_{shear}}, \tag{32}$$

where h_{shear} is a height of a tooth at the end of the contact surface.

If the root is symmetrical and each blade is secured in the individual slot, then tensile stresses at different root sections are calculated as (all indexes and designations are presented in Fig. 18):

$$\sigma_{tens\ bl\ I\ (1)} = \frac{P_{centr\ airfoil} + P_{centr\ plate} + P_{c\,I}}{b_I' \; l_I}, \tag{33}$$

$$\sigma_{tens\ bl\ II\,(1)} = \frac{P_{centr\ airfoil} + P_{centr\ plate} + P_{c\,I} + P_{c\,II} - 2N_1 cos\theta}{b'_{II}\ l_{II}}, \qquad (34)$$

$$\sigma_{tens\ bl\ III\,(1)} = \frac{1}{b'_{III} \cdot l_{III}}\Big(P_{centr\ airfoil} + P_{centr\ plate} + P_{c\,I} + P_{c\,II} + \\ + P_{c\,III} - 2N_1 \cos\theta - 2N_2 \cos\theta, \qquad (35)$$

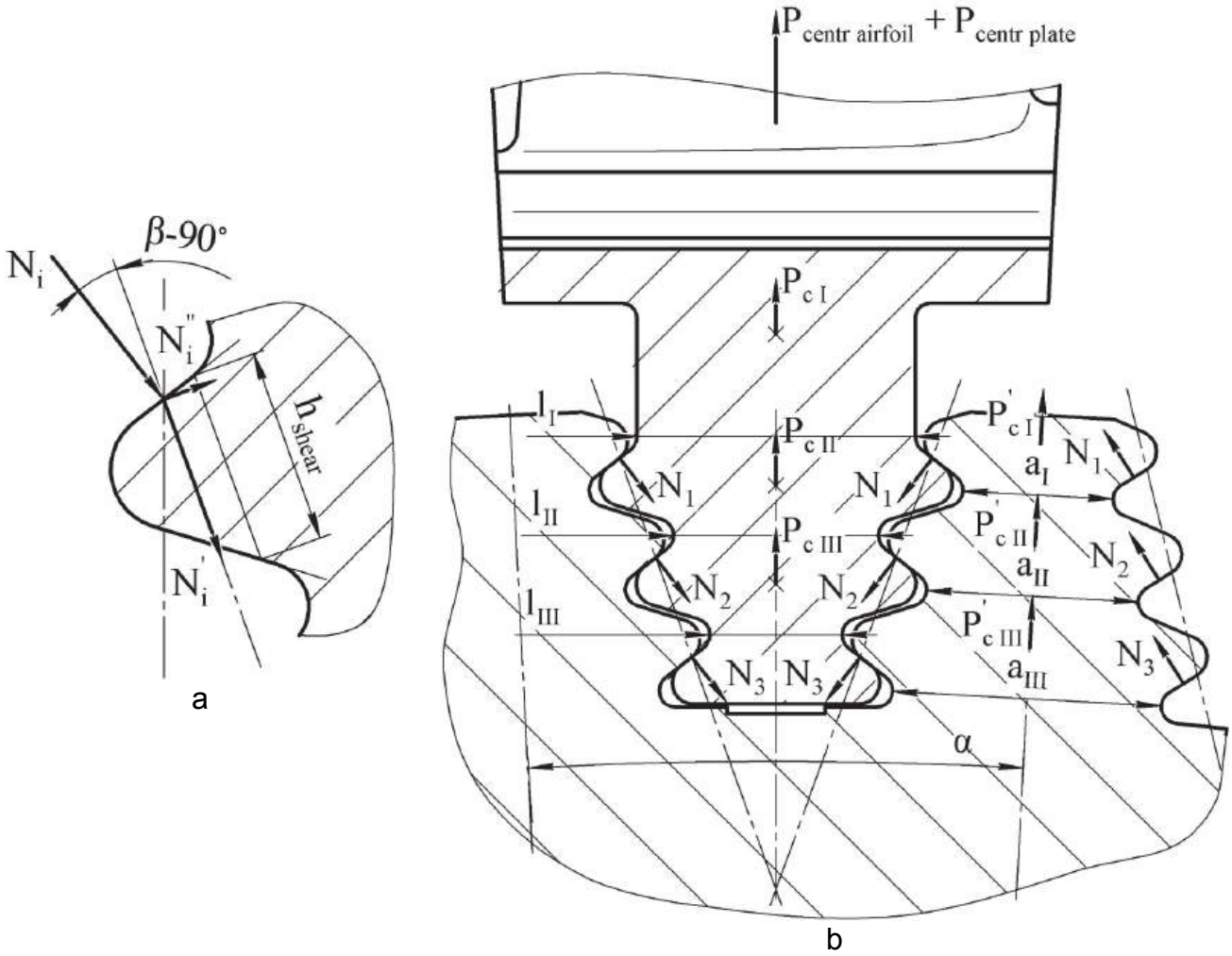

Fig. 18. The design scheme of the fir-tree joint:
a – shearing strength analysis of the tooth;
b – tensile strength analysis of the root and disk rim

or in the general view

$$\sigma_{tens\ bl_q\ (1)} = \frac{P_{centr\ airfoil} + P_{centr\ plate} + \sum_{i=1}^{q} P_{c_i} - 2cos\theta \sum_{i=0}^{q-1} N_i}{b'_i\ l_i}, \qquad (36)$$

where P_{c_i} are centrifugal forces of segments, which are limited by two adjacent design sections (i^{th} and $i\text{-}1^{th}$);

l_i, b_i' are minimum neck width and length of the root respectively; these parameters determine the areas at design sections; b_i' is equal to b in case of constant rim width (see Fig. 16);

q – the number of tooth pairs.

If the chord to pitch ratio of the blade is high, then two blades are fitted in one slot. In this case, the centrifugal forces, generated by airfoil component and shroud plate, must be doubled. Then, equations (33) and (36) are transformed to

$$\sigma_{tens\ bl\ (2)} = 2\frac{P_{centr\ airfoil} + P_{centr\ plate} + P_{c\,l}}{b_l\ l_l}, \tag{37}$$

$$\sigma_{tens\ bl_q\ (2)} = 2\frac{P_{centr\ airfoil} + P_{centr\ plate} + \sum_{i=1}^{q} P_{c_i} - cos\theta \sum_{i=0}^{q-1} N_i}{b_i'\ l_i}, \tag{38}$$

where P_{c_i} are centrifugal forces of segments, which are limited by two adjacent design sections (i^{th} and $i\text{-}1^{th}$); these forces are calculated for one of the blades;

N_i are reactions, which load the teeth (see eq. (26)); they act normal to contact surface.

Maximum stresses in the modern roots are:

- bearing stress – 230 MPa;
- shearing stress – 120 MPa;
- bending and tensile stresses – 200 MPa.

The upper design section I–I (the upper neck) is normally the most loaded.

If the geometrical parameters of root teeth and steeple teeth are the same, then shearing, bending and bearing stresses acting upon them are also the same.

The tensile stress acting upon the disk steeple is generated as by root teeth, so by steeple elements. The stress is calculated as

$$\sigma_{tens\ steeple\,l} = \frac{2N_1 cos\left(\theta + \frac{\alpha}{2}\right) + P_{c\,l}'}{a_l \cdot b''_l}, \tag{39}$$

$$\sigma_{tens\ steeple\ II} = \frac{2\left(N_1 + N_2\right)\cos\left(\theta + \frac{\alpha}{2}\right) + P'_{c\,I} + P'_{c\,II}}{a_{II}\ b''_{II}}, \qquad (40)$$

$$\sigma_{tens\ steeple\ III} = \frac{2\left(N_1 + N_2 + N_3\right)\cos\left(\theta + \frac{\alpha}{2}\right) + P'_{c\,I} + P'_{c\,II} + P'_{c\,III}}{a_{III}\ b''_{III}}, \qquad (41)$$

or in the general view

$$\sigma_{tens\ steeple_q} = \frac{2\cos\left(\theta + \frac{\alpha}{2}\right) \cdot \sum_{i=1}^{q} N_i + \sum_{i=1}^{q} P'_{c_i}}{a_i\ b''_i}, \qquad (42)$$

where P'_{c_i} are centrifugal forces of steeple segments, which are limited by two adjacent design sections;

$\alpha = 360°/z$ – angle between axes of adjacent blades;

z – the number of blades;

a_i, b''_i – width and length of the steeple necks.

Maximum tensile stress in the disk rim originates at the neck of the steeple. Maximum values are equal to 230 MPa.

Besides, the sections of the upper neck (I–I) of the blade root and the bottom neck (III–III) of the disk (see Fig. 18) are also stressed by bending generated by momentum of gas forces and inertia.

The presented stresses normally generated in fir-tree roots belong to maximum stresses, which are calculated by formulas. The real stresses may be 2.5…3.5 times higher due to stress concentration at tooth base. Besides all above mentioned, variable in time gas loads acting the blade generate vibration stress in roots. Fatigue cracks mostly appear right above the upper teeth of the blade root.

5. EXAMPELES OF ROOT ANALYSIS

5.1. The analysis of the dovetail root

Task: Make the checking strength analysis of the dovetail joint. Compressor blade and disk are made of titanium alloy. The design scheme of the root is presented in Fig. 19. The acting loads and the geometrical parameters are presented in Table 4.

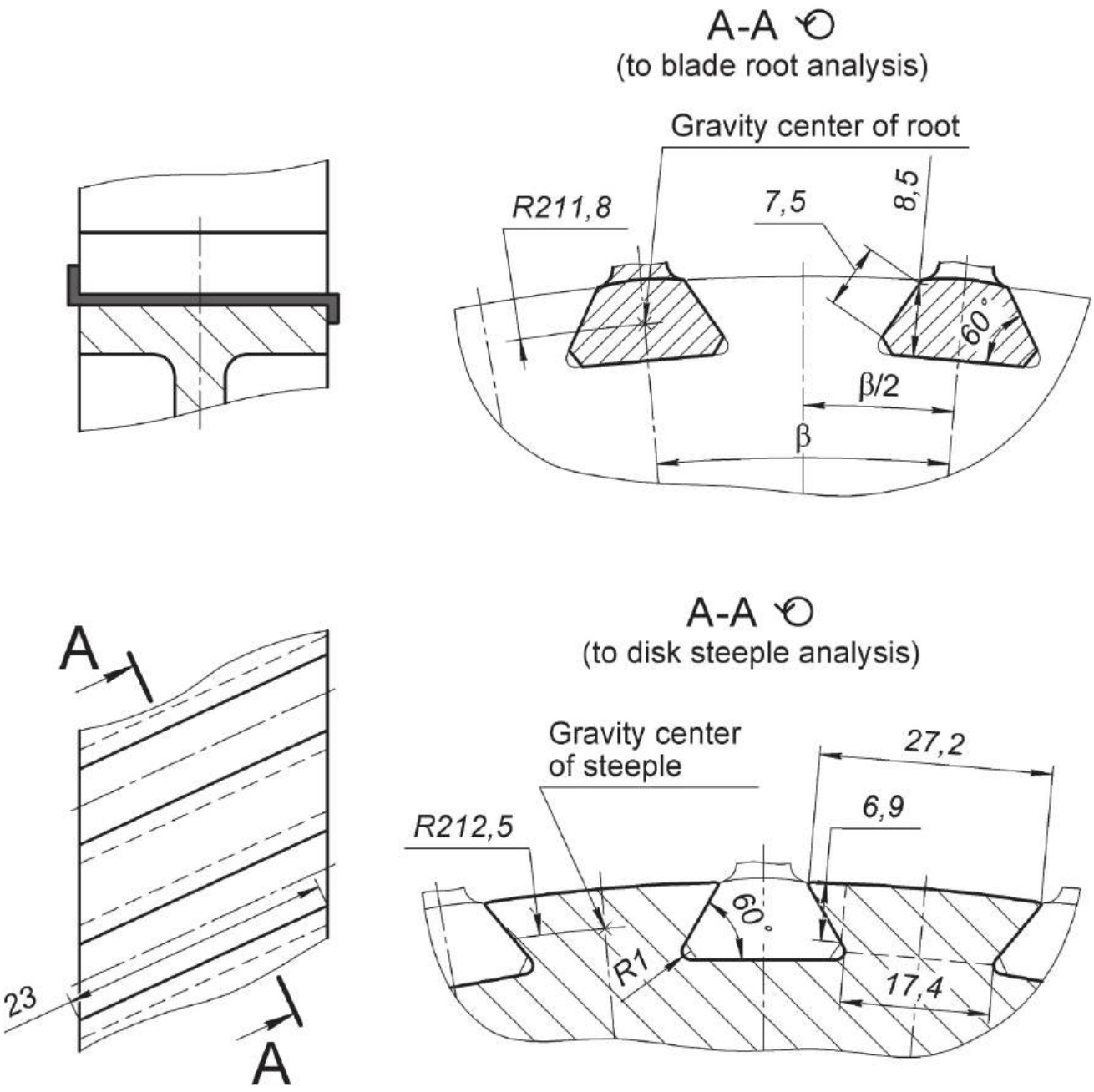

Fig. 19. Geometrical parameters of the dovetail joint

Table 4. Initial data for the dovetail joint analysis

Parameter	Designation	Value	Measuring unit
Number of impeller blades	z	**36**	*pcs*
Density of material blade and disk are made of	ρ	**4530**	kg/m^3
Coefficient of sliding friction of titanium alloy	f	**0.5**	-
Rotational speed	n	**10670**	*rpm*
Tensile stress at root section of the blade	$\sigma_{tens\ root}$	**138.9**	*MPa*
Area of the root section	F_{root}	$\mathbf{1.07 \cdot 10^{-4}}$	m^2
Flank angle of the root	α	**60**	*deg*
Angle between slot floor and the axis of rotation	ψ	**0**	*deg*
Slot length	b	**0.023**	*m*
The radius of the root gravity center	$R_{g.c.\ root}$	**0.2118**	*m*
The radius of the steeple gravity center	$R_{g.c.\ steeple}$	**0.2125**	*m*
The width of the contact spot	C	**0.0075**	*m*
The width of shear area of the root	h_{II}	**0.0085**	*m*
The width of shear area of the steeple	h_{III}	**0.0069**	*m*
Neck width of the steeple	a	**0.0174**	*m*
Steeple width at the outer radius of the disk	B	**0.0272**	*m*
Radius of a rounding arc or dimensions of a chamfer at the slot floor	r	**0.001**	*m*

The analysis order

1. Get additional initial data.

Angular speed of rotor

$$\omega = \frac{2\pi n}{60} = \frac{\pi n}{30} = \frac{\pi \cdot 10670}{30} = 1117 \ \text{s}^{-1}.$$

Mass of the blade root

$$m_{root} = V_{root}\rho = F_{root}b\rho,$$

where V_{root} is the root volume;

F_{root} area of a transversal section of the root (see Fig. 19).

Draw the full-scale dovetail joint according to the given dimensions and measure the needed geometrical parameter of the section.

Hence, the measured area of the transversal section of the root is $F_{root} = 1.35 \cdot 10^{-4}\ m^2$. Then, the mass of the root is

$$m_{root} = 1.35 \cdot 10^{-4} \cdot 0.023 \cdot 4530 = 14.07 \cdot 10^{-3} \text{ kg.}$$

The mass of the steeple

$$m_{steeple} = V_{steeple}\rho = F_{steeple}b\rho,$$

where $V_{steeple}$ is the volume of the steeple;
$F_{steeple}$ is the area of the transversal section of the steeple (see Fig. 19).

The measured area of the transversal section of the steeple is $F_{steeple} = 1.793 \cdot 10^{-4}\ m^2$. Then the mass of the steeple is

$$m_{steeple} = 1.793 \cdot 10^{-4} \cdot 0.023 \cdot 4530 = 18.65 \cdot 10^{-3} \text{ kg.}$$

The angle between the adjacent slots (see Fig. 19) equals to:

$$\beta = \frac{360^\circ}{z} = \frac{360^\circ}{36} = 10^\circ.$$

2. Calculate forces, which are components of equation (1):
   - centrifugal force of airfoil

$$P_{centr\ airfoil} = \sigma_{tens\ root} \cdot F_{root\ airfoil} = 138.9 \cdot 10^6 \cdot 1.07 \cdot 10^{-4} = 14860 \text{ N;}$$

   - centrifugal force of root

$$P_{centr\ root} = m_{root} R_{g.c\ root} \omega^2 = 14.07 \cdot 10^{-3} \cdot 0.2118 \cdot 1117^2 = 3870 \text{ N;}$$

   - total centrifugal force of the blade

$$P_{centr\ bl} = P_{centr\ airfoil} + P_{centr\ root} = 14860 + 3870 = 18730 \text{ N.}$$

3. Calculate the reaction (3), which acts the contact surfaces of the root:

$$N = \frac{P_{centr\ bl} \cos\psi}{2(\cos\alpha + f \sin\alpha)} = \frac{18730 \cdot 1}{2(0.5 + 0.5 \cdot 0.866)} = 10038 \text{ N.}$$

4. Calculate the bearing stress by the formula (4):

$$\sigma_{bear} = \frac{N}{c\ b} = \frac{10038}{0.0075 \cdot 0.023} = 58.2 \text{ MPa}.$$

5. Calculate the centrifugal force of the steeple:

$$P_{centr\ steeple} = m_{steeple} R_{g.c.\ steeple} \omega^2 = 18.65 \cdot 10^{-3} \cdot 0.2125 \cdot 1117^2 = 4944 \text{ N}.$$

6. Calculate the tearing force Q, which acts the steeple, by formula (6):

$$Q = 2N\cos\left(\alpha - \frac{\beta}{2}\right) + P_{centr\ steeple} = 2 \cdot 10038 \cdot 0.5736 + 4944 = 16460 \text{ N}.$$

7. Calculate the tensile stress at the neck section of the steeple by the formula (5):

$$\sigma_{tens} = \frac{Q}{a\ b} = \frac{16460}{0.0174 \cdot 0.023} = 41 \text{ MPa}.$$

8. Determine the stress concentration factor (Fig. 20). Use radius of rounding arc r at the slot floor, parameters a and B of the steeple and diagrams, presented at Fig. 14, as initial data.

$$\frac{B}{a} = \frac{0.0272}{0.0174} = 1.56 \approx 1.5; \quad \frac{r}{a} = \frac{0.001}{0.0174} = 0.057 \approx 0.06.$$

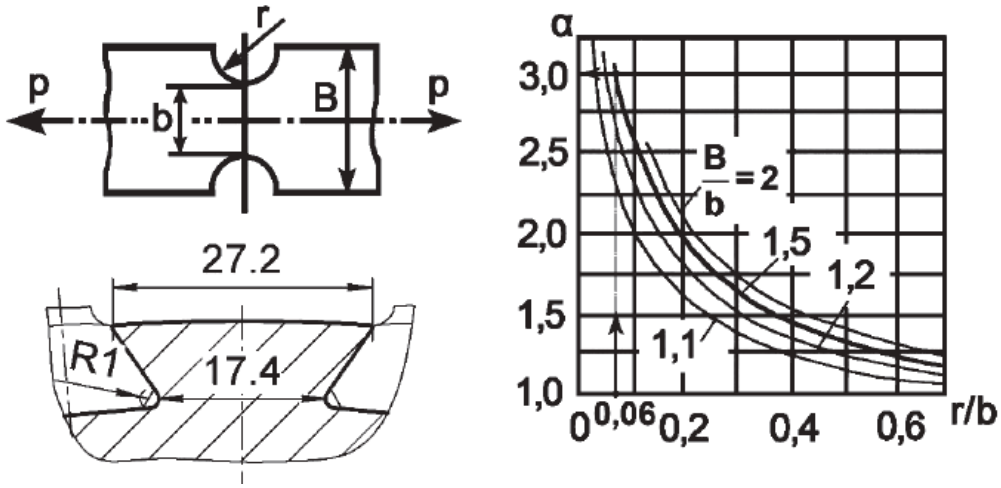

Fig. 20. Diagrams for determination of the stress concentration factor

Then, the stress concentration factor was determined to be a_{conc} = 3.0.
True stress at the steeple neck is

$$\sigma_{tens\ max} = a_{conc}\sigma_{tens} = 3.0 \cdot 41 = 123 \text{ MPa.}$$

9. Calculate shearing stress generated in the blade root by the equation (8):

$$\tau_{shear\ II} = \frac{P_{centr\ bl}}{2h_{II}b} = \frac{18730}{2 \cdot 0.0085 \cdot 0.023} = 47.9 \text{ MPa.}$$

10. Calculate shearing stress that arises in the steeple of the disk by the formula (9):

$$\tau_{shear\ III} = \frac{P_{centr\ bl}}{2h_{III}b} = \frac{18730}{2 \cdot 0.0069 \cdot 0.023} = 59 \text{ MPa.}$$

11. Compare each calculated stress with the corresponding stress in the modern dovetail roots (see Table 3). Calculate safety factors for each stress. Use

- yield stress σ_y (for the elastic materials);
- 0.2% offset yield stress $\sigma_{0.2}$ (for the brittle materials, which do not have yielding or perfect plasticity),

as an admissible stress.

The temperature of material plays considerable role for the roots of the last compressor stages. So the temperature effect must be considered, when calculating the safety factors. Then admissible stresses must be lowered:

$$k_{tens} = \frac{[\sigma_{0.2}]}{\sigma_{centr\ max}} = \frac{1150}{123} = 9.3; \qquad k_{shear\ II} = \frac{[\sigma_{0.2}]}{\tau_{shear\ II}} = \frac{1150}{47.9} = 24;$$

$$k_{shear\ III} = \frac{[\sigma_{0.2}]}{\tau_{shear\ III}} = \frac{1150}{59} = 19.5.$$

The analysis of the calculated safety factors reveals that:

– all safety factors are more than **3**, which means that the designed dovetail joint meets the Norms of Strength;

– the most dangerous stress is the tensile stress acting the steeple neck, because this safety factor is minimal $k_{tens} = 9.3$;

– the stress state of the root can be improved by increasing the radius of the rounding arc at the slot floor;

– the safety factors are too high to be optimal. This proves that the construction of the joint must be optimized by the decrease of a slot length and

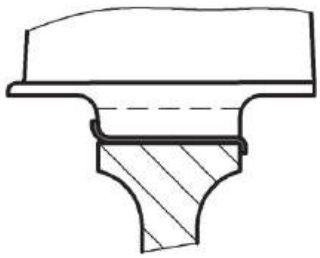

Fig. 21. Recommended modification of dovetail joint

the corresponding decrease of a root length. This gives an opportunity to create the disk with the smaller and lighter rim part (Fig. 21). This also improves the stress state of the disk, because of lower centrifugal forces acting it.

5.2. The analysis of the pinned root

Task: Make the checking strength analysis of the pinned joint. Compressor blade and disk are made of titanium alloy, and a pin is made of heavily alloyed steel. The design scheme of the root is presented in Fig. 15. The acting loads and the geometrical parameters are presented in Table 5 and in Fig. 22.

Table 5. Initial data for the pinned joint analysis

Parameter	Design.	Value	Measuring unit
Number of impeller blades	z	25	*pcs*
Density of material blade and disk are made of	ρ	4530	kg/m^3
Density of material pin is made of	ρ	7800	kg/m^3
Elastic modulus of material blade and disk are made of	E_1	$1.15 \cdot 10^5$	*MPa*
Elastic modulus of material pin is made of	E_2	$2 \cdot 10^5$	*MPa*
Poisson`s ratio (*is considered equal for all materials*)	μ	0.3	---
Rotational speed	n	10750	*rpm*
Tensile stress at root section of the blade	$\sigma_{tens\ root}$	149.3	*MPa*
Area of the blade root section	F_{root}	$2.09 \cdot 10^{-4}$	m^2
Mass of the root sector, which is above the section A-A	m_2	0.038	*kg*
Mass of the root	m_x	0.052	*kg*
Mass of the pin	m_3	0.023	*kg*
Total mass of the disk sector «***a-b-c-d-e-f***»	m_4	0.048	*kg*
Total mass of the disk sector «***a-b-c-d***»	m_5	0.006	*kg*
Mass of the pin sectors, which are inside the root	m_6	0.013	*kg*
Gravity center radius of the root sector, which is above the pin hole axis	$R_{g.c.2}$	0.112	*m*
Gravity center radius of the root	$R_{g.c.\ root}$	0.108	*m*
Gravity center radius of the disk sector «***a-b-c-d-e-f***»	$R_{g.c.\ 4}$	0.107	*m*
Gravity center radius of the disk sector «***a-b-c-d***»	$R_{g.c.\ 5}$	0.109	*m*
Diameter of the circle, which is set of all hole centers in a plane that are at a given distance from the axis of rotation	$D_{h\ rim}$	0.2	*m*

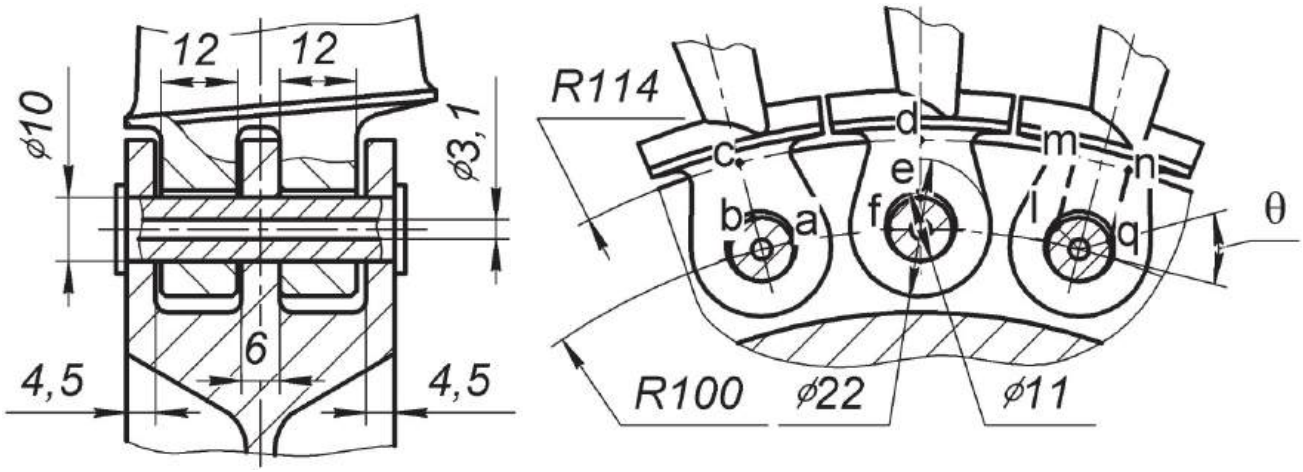

Fig. 22. Dimensions of pinned joint

The analysis order

1. Get additional initial data.

Angular speed of rotor

$$\omega = \frac{2\pi n}{60} = \frac{\pi n}{30} = \frac{\pi \cdot 10750}{30} = 1125 \text{ s}^{-1};$$

2. Calculate the centrifugal forces, which load the elements of joint by formulas (21), (22):

- centrifugal force of the blade airfoil

$$P_{centr\ airfoil} = \sigma_{tens\ root\ airfoil} F_{root\ airfoil} = 149.3 \cdot 10^6 \cdot 2.09 \cdot 10^{-4} = 31204 \text{ N};$$

- centrifugal force of the root sector, which is above the section A-A

$$P_{centr_2} = m_2 R_{centr_2} \omega^2 = 0.038 \cdot 0.112 \cdot 1125^2 = 5386.5 \text{ N};$$

- centrifugal force of the whole root

$$P_{centr\ root} = m_{root} R_{g.c.\ root} \omega^2 = 0.052 \cdot 0.108 \cdot 1125^2 = 7108 \text{ N};$$

- centrifugal force of the pin

$$P_{centr_3} = m_3 \frac{D_{h\ rim}}{2} \omega^2 = 0.023 \cdot \frac{0.2}{2} \cdot 1125^2 = 2911 \text{ N};$$

- total centrifugal force of the disk sector «***a-b-c-d-e-f***»

$$\sum_{i=1}^{3}\left(P_{centr_4}\right)_i = m_4 R_{g.c._4}\omega^2 = 0.048 \cdot 0.107 \cdot 1125^2 = 5823 \text{ N};$$

– total centrifugal force of the disk sector «***a-b-c-d***»

$$\sum_{i=1}^{3}\left(P_{centr_5}\right)_i = m_5 R_{g.c._5}\omega^2 = 0.006 \cdot 0.109 \cdot 1125^2 = 828 \text{ N};$$

– total centrifugal force of an equivalent length pin (the equivalent length is equal to the sum of root portion widths

$$P_{centr_6} = m_6 \frac{D_{h\,rim}}{2}\omega^2 = 0.013 \cdot \frac{0.2}{2} \cdot 1125^2 = 1645 \text{ N}.$$

3. Calculate tensile stress acting section A-A of the root portion. Use the formula (10):

$$\sigma_{tens\ bl} = \frac{P_{centr\ airfoil} + P_{centr_2}}{(D-d)\sum_{i=1}^{k} b_i} = \frac{31204 + 5386.5}{(0.022 - 0.011)\cdot(0.012 + 0.012)} = 139 \text{ MPa}.$$

4. Calculate contact line length distributed load by the formula (12):

$$p = \frac{P_{centr\ bl}}{\sum_{i=1}^{k} b_i} = \frac{31204 + 7108}{2 \cdot 0.012} = 1.6 \cdot 10^6 \text{ N/m}.$$

5. Determine the maximum contact stress acting the joint by the formula (11):

$$\sigma_{contact} = 0.798\sqrt{p\frac{d - d_{pin}}{d\ d_{pin}}\frac{E_1 E_2}{\left(1-\mu^2\right)\left(E_1 + E_2\right)}} =$$

$$= 0.798\sqrt{\frac{1.6 \cdot 10^6 \cdot \frac{0.011 - 0.01}{0.011 \cdot 0.01}}{\left(1 - 0.3^2\right)} \cdot \frac{1.15 \cdot 10^{11} \cdot 2 \cdot 10^{11}}{1.15 \cdot 10^{11} + 2 \cdot 10^{11}}} = 862 \text{ MPa}.$$

6. Calculate the tensile stress at the weakness section of the platform portion (the axys of holes for pins form to the weakness section) by the formula (13)

$$\sigma_{tens\ p.p} = \frac{P_{centr\ \Sigma}}{F_{rim}} = \frac{P_{centr\ \Sigma}}{\left(\frac{\pi}{z} D_{h\ rim} - d_h\right) \sum_{i=1}^{s} \left(b_{p.p}\right)_i} =$$

$$= \frac{37183 + 2911 + 5823}{\left(\frac{\pi}{25} \cdot 0.2 - 0.01\right) \cdot 0.015} = 202.3 \text{ MPa.}$$

7. Calculate the bearing stress that arise between the root portion and the pin by formula (15)

$$\sigma_{bear\ \ root\ portion} = \frac{P_{centr\ bl}}{d_{pin} \sum_{i=1}^{k} b_i} = \frac{37183}{0.01 \cdot 0.024} = 154.9 \text{ MPa.}$$

8. Calculate the bearing stress that arise between the pin and the platform portion by formula (16)

$$\sigma_{bear\ platf\ portion} = \frac{P_{centr\ \ bl} + P_{centr\ pin}}{d_{pin} \sum_{i=1}^{s} \left(b_{platf\ portion}\right)_i} = \frac{37183 + 2911}{0.01 \cdot 0.015} = 267.3 \text{ MPa.}$$

9. Calculate the total shearing force by the formula (19)

$$P_{shear\ \Sigma} = P_{centr\ \ bl} + P_{centr\ \ pin} + \sum_{i=1}^{s} \left(P_{centr_5}\right)_i = 37183 + 2911 + 828 = 40922 \text{ N.}$$

10. Calculate the angle, which limits the shearing sector in the platform portions. Use the formula (18):

$$\theta = \arcsin\left(\frac{d_{pin}}{2h}\right) = \arcsin\left(\frac{0.01}{0.014}\right) = 45.6°.$$

11. Calculate the shearing stress in the disk rim by the formula (17):

$$\tau_{shear\ \ platf\ portion} = \frac{P_{shear\ \Sigma} \cos\theta}{\left(2h - d_{pin} \sin\theta\right) \sum_{i=1}^{s} \left(b_{platf\ portion}\right)_i} =$$

$$= \frac{40922 \cdot \cos 45.6°}{\left(2 \cdot 0.014 - 0.01 \cdot \sin 45.6°\right) \cdot 0.015} = 91.5 \text{ MPa.}$$

12. Calculate the shearing stress in the pin by the formula (20)

$$\tau_{shear\ pin} = \frac{P_{centr\ bl} + P_{centr_6}}{\frac{\pi}{4} n_0 \left(d_{pin}^2 - d_{app}^2\right)} = \frac{37183 + 1645}{\frac{3.14}{4} \cdot 4 \cdot \left(0.01^2 - 0.0031^2\right)} = 136.7 \text{ MPa.}$$

13. Compare each calculated stress with the corresponding stress in the modern dovetail roots (see Table 4).

The safety factor for each part can be determined by the loading that causes maximum stress:

- by the contact stress in the joint

$$k_{contact} = \frac{\left[\sigma_{0.2}\right]}{\sigma_{contact}} = \frac{1150}{862} = 1.33 \text{ ;}$$

- by the bearing stress, which arises at contact surfaces of the pin and the blade root

$$k_{bear\ root} = \frac{\left[\sigma_{0.2}\right]}{\sigma_{bear\ root}} = \frac{1150}{154.9} = 7.4 \text{ ;}$$

- by the bearing stress at the contact surfaces of the pin and the disk

$$k_{bear\ disk} = \frac{\left[\sigma_{0.2}\right]}{\sigma_{bear\ disk}} = \frac{1150}{267.3} = 4.3 \text{ ;}$$

- by the shearing stress in the pin

$$k_{shear\ pin} = \frac{\left[\sigma_{0.2}\right]}{\sigma_{shear\ pin}} = \frac{850}{136.7} = 6.2 \text{ .}$$

The analysis of the calculated safety factors reveals that:

1. The designed pinned joint does not meet the requirements presented in the Norms of Strength, because the safety factor on contact stress is less than ***3*** (***$k_{contact}$ = 1.33 < 3***). Besides, the contact stress is ***7.8%*** higher than stresses that arise in the modern pinned roots (see Table 4).

2. The rest safety limits meet the requirements of the Norms of Strength. The most dangerous are the bearing stress at the contact surfaces of the pin and the disk, because the safety factor is minimum (***$k_{bear\ disk}$ = 4.3 > 3***);

3. To meet the requirements made by the Norms of Strength the designer must change the construction. The clearance between the pin and the platform, and the pin and the root must be reduced.

5.3. The analysis of the fir-tree root

Task: Make the checking strength analysis of the fir-tree joint. Two turbine blades are mounted in one slot, so the blade belongs to twin blades. The design scheme of the root is presented in Fig. 15. The acting loads and the geometrical parameters are presented in Table 6.

Tensile stress, bending stress and shearing stress that arise in each tooth must be approximately equal. In this case the root is considered perfectly designed. The main goal of the checking strength analysis is the verification of geometrical parameters of the root. Hence, the analysis must be performed for all tooth pairs.

Table 6. Initial data for the fir-tree joint analysis

Parameter	Designation	Value	Measuring unit
Number of impeller blades	z	118	*pcs*
Density of material blade and disk are made of	ρ	8200	kg/m^3
Rotational speed	n	13800	*rpm*
Tensile stress at root section of the blade	$\sigma_{tens\ root}$	225.5	*MPa*
Area of the root section	F_{root}	$1.23 \cdot 10^{-4}$	m^2
Length of the contact surface of the i^{th} tooth pair	b_1 $b_2 = b_3$	0.0266 0.028	*m*
Width of the stress area	c	0.002	*m*
Wedge angle of the tooth slot (blade root)	φ	40	*deg*
Angle between “wedge” line and a normal to the contact surface of the tooth	β	105	*deg*
Angle between contact and non-contact surface of the tooth	γ	55	*deg*

Continuation of the Table 6

Arm of reaction, which bends the tooth	e	0.0009	*m*
Height of tooth base that works in bending	h_{bend}	0.0042	*m*
Height of tooth base that works in shearing	H_{shear}	0.0039	*m*
Minimum neck width of the ith tooth pair of the root	l_1 l_2 l_3	0.0138 0.0103 0.0068	*m*
Minimum neck width of the ith tooth pair of the steeple	a_1 a_2 a_3	0.009 0.012 0.0151	*m*
Mass of the shroud plate	m_{plate}	0.0034	*kg*
Gravity center radius of the shroud plate	$R_{g.c.\ plate}$	0.317	*m*
Mass of the root sector	m_I m_{II} m_{III}	0.0292 0.0083 0.0069	*kg*
Gravity center radius of the root sector	$R_{g.c.\ I}$ $R_{g.c.\ II}$ $R_{g.c.\ III}$	0.26 0.25 0.245	*m*
Mass of the steeple sector	m'_I m'_{II} m'_{III}	0.0088 0.0147 0.0181	*kg*
Gravity center radius of the steeple sector	$R'_{g.c.\ I}$ $R'_{g.c.\ II}$ $R'_{g.c.\ III}$	0.252 0.2477 0.2428	*m*

The analysis order

1. Get additional initial data:
   - angular speed of rotor

$$\boldsymbol{\omega} = \frac{\boldsymbol{2\pi\, n}}{\boldsymbol{60}} = \frac{\boldsymbol{\pi\, n}}{\boldsymbol{30}} = \frac{\boldsymbol{\pi \cdot 13800}}{\boldsymbol{30}} = \boldsymbol{1444}\ \text{s}^{-1};$$

   - angle between axes of adjacent slots (see Fig. Fig. **19**):

$$\boldsymbol{\alpha} = \frac{\boldsymbol{360}^\circ}{\boldsymbol{z}} = \frac{\boldsymbol{360}^\circ}{\boldsymbol{118}} = \boldsymbol{3.051}^\circ;$$

   - angle between the contact surface and the symmetry plane of the tooth (see Fig. 17, a):

$$\boldsymbol{\theta} = \frac{\boldsymbol{\varphi}}{\boldsymbol{2}} + \left(\boldsymbol{\beta} - \boldsymbol{90°}\right) = \frac{\boldsymbol{40°}}{\boldsymbol{2}} + \left(\boldsymbol{105°} - \boldsymbol{90°}\right) = \boldsymbol{35°}.$$

2. Calculate forces acting segments of fir-tree root. This calculation is done in the same manner to the strength analysis of the pinned root:

– centrifugal force of the airfoil

$$P_{\text{centr airfoil}} = \sigma_{tens} F_{airfoil\ root} = 225.5 \cdot 10^6 \cdot 1.23 \cdot 10^{-4} = 27737 \text{ N};$$

– centrifugal force of the shroud plate

$$P_{\text{centr plate}} = m_{plate} R_{g.c.\ plate} \omega^2 = 0.0034 \cdot 0.317 \cdot 1444^2 = 2247 \text{ N};$$

– centrifugal forces of root segments, which are limited by two adjacent design sections (see Fig. 18):

$$P_{centr\ I} = m_I R_{g.c.\ I} \omega^2 = 0.0292 \cdot 0.26 \cdot 1444^2 = 15830 \text{ N};$$

$$P_{centr\ II} = m_{II} R_{g.c.\ II} \omega^2 = 0.0083 \cdot 0.25 \cdot 1444^2 = 4327 \text{ N};$$

$$P_{centr\ III} = m_{III} R_{g.c.\ III} \omega^2 = 0.0069 \cdot 0.245 \cdot 1444^2 = 3525 \text{ N};$$

– centrifugal forces of steeple segments, which are limited by two adjacent design sections (see Fig. 18):

$$P'_{centr\ I} = m'_I R'_{g.c.\ I} \omega^2 = 0.0088 \cdot 0.252 \cdot 1444^2 = 4624 \text{ N};$$

$$P'_{centr\ II} = m'_{II} R'_{g.c.\ II} \omega^2 = 0.0147 \cdot 0.2477 \cdot 1444^2 = 7592 \text{ N};$$

$$P'_{centr\ III} = m'_{III} R'_{g.c.\ III} \omega^2 = 0.0181 \cdot 0.2428 \cdot 1444^2 = 9113 \text{ N};$$

– centrifugal force of entire blade

$$P_{centr\ bl} = P_{centr\ airfoil} + P_{centr\ plate} + P_{centr\ I} + P_{centr\ II} + P_{centr\ III} =$$
$$= 27737 + 2247 + 15830 + 4327 + 3525 = 53666 \text{ N}.$$

3. Calculate the reaction, which acts the i^{th} tooth of the root by the formula (26):

$$N_1 = \frac{P_{centr\ bl}}{\cos\theta}\frac{b_i}{\sum_{i=1}^{n} b_i} = \frac{53666}{0.8192}\cdot\frac{0.0266}{(0.0266 + 2\cdot 0.028)} = 21094 \text{ N};$$

$$N_2 = N_3 = \frac{53666}{0.8192}\cdot\frac{0.028}{(0.0266 + 2\cdot 0.028)} = 22207 \text{ N}.$$

4. Calculate the bearing stress that is generated at the contact surface of the i^{th} tooth (Fig. 23, a) by the formula (27):

$$\sigma_{bear\ 1} = \frac{P_{bear\ 1}}{F_{bear\ 1}} = \frac{N_1}{c\,b_1} = \frac{21094}{0.002\cdot 0.0266} = 396.5 \text{ MPa};$$

$$\sigma_{bear\ 2,3} = \frac{P_{bear\ 2,3}}{F_{bear\ 2,3}} = \frac{N_{2,3}}{c\,b_{2,3}} = \frac{22207}{0.002\cdot 0.028} = 396.6 \text{ MPa}.$$

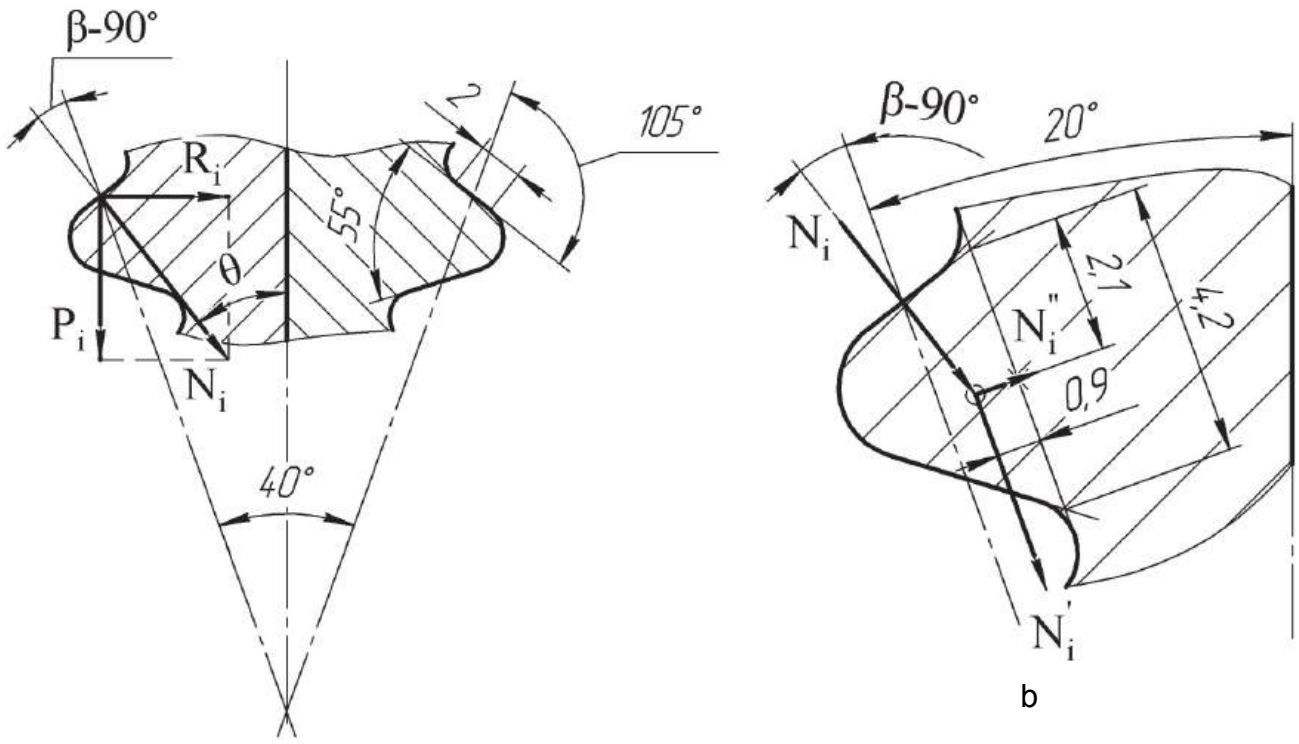

Fig. 23. The design scheme of the fir-tree joint:
a – bearing strength analysis of the tooth; b – bending strength analysis of the tooth

5. Calculate the bending stress originating at the base of the i^{th} tooth (Fig. 23, b) by the formula (31):

$$\sigma_{bend\ 1} = \frac{6N_1\, e \cos(\beta - 90°)}{b_1\, h_{bend}^2} = \frac{6 \cdot 21094 \cdot 0.0009 \cdot 0.966}{0.0266 \cdot 0.0042^2} = 234.6 \text{ MPa};$$

$$\sigma_{bend\ 2,3} = \frac{6N_{2,3}\, e \cos(\beta - 90°)}{b_{2,3}\, h_{bend}^2} = \frac{6 \cdot 22207 \cdot 0.0009 \cdot 0.966}{0.028 \cdot 0.0042^2} = 249.7 \text{ MPa}.$$

6. Calculate maximal shearing stress at the base of the i^{th} tooth (Fig. 24) by the formula (32):

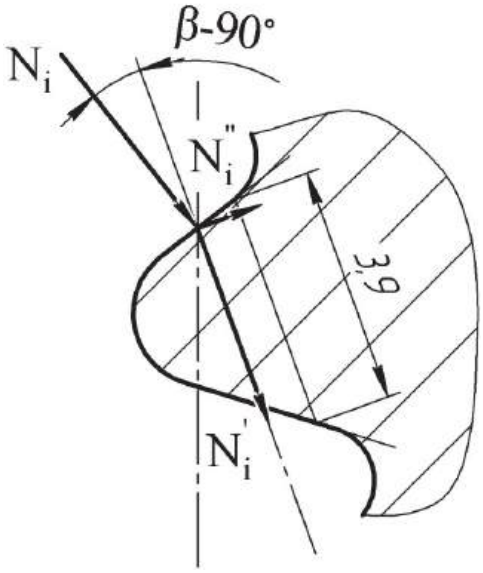

Fig. 24. The design scheme for the determination of shearing stress

$$\tau_{shear\ 1} = \frac{P_{shear\ 1}}{F_{shear\ 1}} = \frac{N_1 \cos(\beta - 90°)}{b_1\, h_{shear}} = \frac{21094 \cdot 0.966}{0.0266 \cdot 0.0039} = 212.8 \text{ MPa};$$

$$\tau_{shear\ 2,3} = \frac{P_{shear\ 2,3}}{F_{shear\ 2,3}} = \frac{N_{2,3} \cos(\beta - 90°)}{b_{2,3}\, h_{shear}} = \frac{22207 \cdot 0.966}{0.028 \cdot 0.0039} = 196.4 \text{ MPa}.$$

7. Calculate tensile stress that appear at the i^{th} root neck (Fig. 25). Use the formulas (37) and (38) for the twin root:

$$\sigma_{tens\ I\ (2)} = 2\frac{P_{centr\ airfoil} + P_{centr\ plate} + P_{centr\ I}}{f_I \cdot l_I} =$$

$$= 2 \cdot \frac{27737 + 2247 + 15830}{0.0266 \cdot 0.0138} = 249.6 \text{ MPa};$$

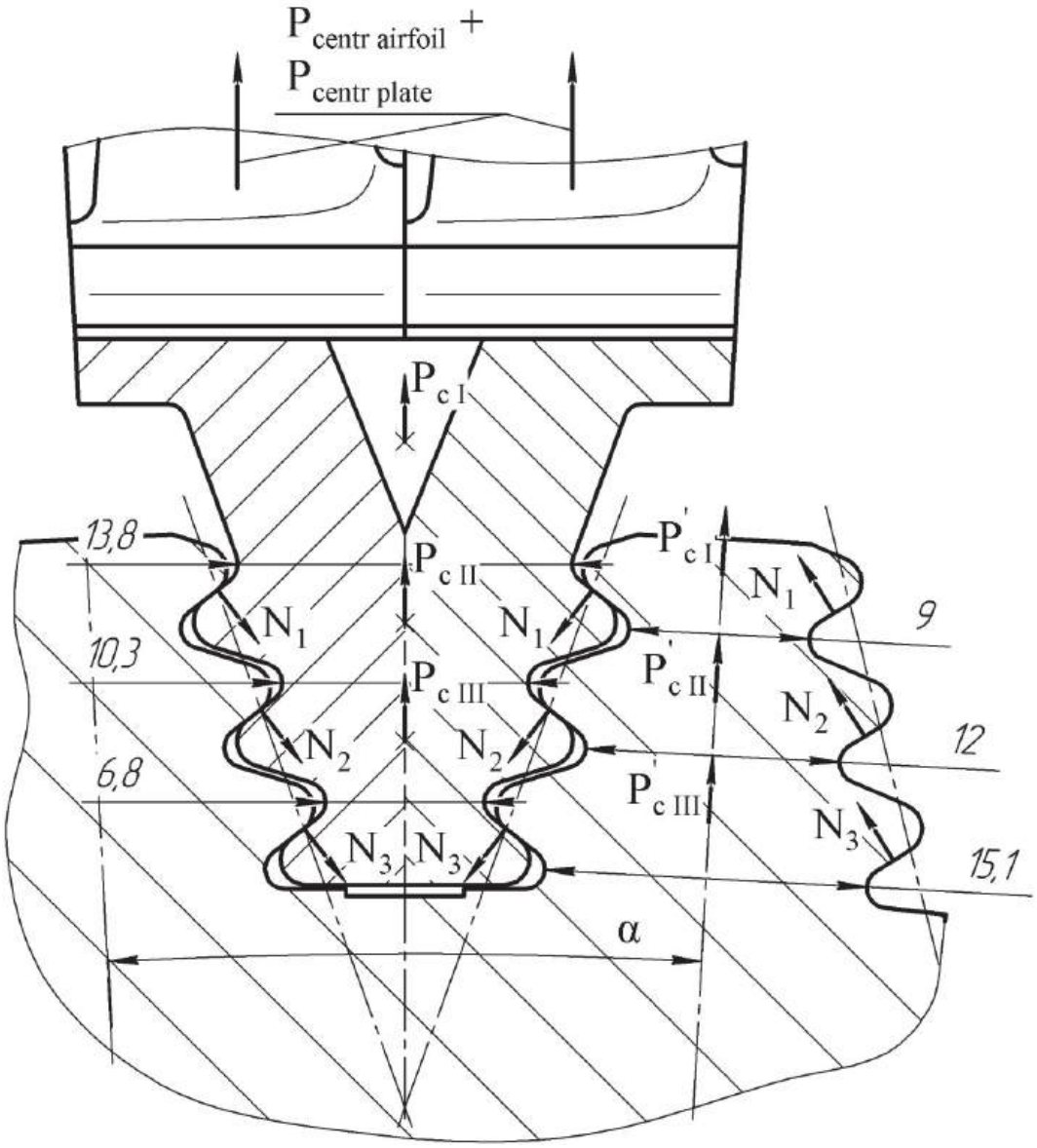

Fig. 25. The design scheme for the determination of tensile stress

$$\sigma_{tens\ II\ (2)} = \sigma_{tens\ n\ (2)} = 2\frac{P_{centr\ airfoil} + P_{centr\ plate} + \sum_{i=1}^{n} P_{c_i} - \sum_{i=0}^{n-1} N_i \cos\theta}{f_i\, l_i} =$$

$$= 2\frac{27737 + 2247 + 15830 + 4327 - 21094 \cdot 0.819}{0.028 \cdot 0.0103} = 227.9 \text{ MPa};$$

$$\sigma_{tens\ III\ (2)} = \sigma_{tens\ n\ (2)} = 2\frac{P_{centr\ airfoil} + P_{centr\ plate} + \sum_{i=1}^{n} P_{c_i} - \sum_{i=0}^{n-1} N_i \cos\theta}{f_i\, l_i} =$$

$$= 2\left(\frac{27737 + 2247 + 15830 + 4327 + 3525}{0.0266 \cdot 0.0068} - \right.$$

$$\left. - \frac{0.819\left(21094 + 22207\right)}{0.0266 \cdot 0.0068} \right) = 191.2 \text{ MPa.}$$

8. Calculate the tensile stress that appear at the i^{th} steeple neck by the formulas (39), (42). Areas of steeple necks are accepted equal to the corresponding areas of the root necks ($d_i = b_i$) to simplify the analysis. Hence

$$\sigma_{tens\ 1} = \frac{2N_1 \cos\left(\theta + \frac{\alpha}{2}\right) + P'_{c\,I}}{a_1 b_1} = \frac{2 \cdot 21094 \cdot 0.8036 + 4624}{0.009 \cdot 0.0266} = 160.5 \text{ MPa;}$$

$$\sigma_{tens\,2} = \frac{2N_2 \cos\left(\theta + \frac{\alpha}{2}\right) + P'_{c\,I} + P'_{c\,II}}{a_2 b_2} =$$

$$= \frac{2 \cdot \left(21094 + 22207\right) \cdot 0.8036 + 7592 + 4624}{0.012 \cdot 0.028} = 205.4 \text{ MPa;}$$

$$\sigma_{tens\,3} = \frac{2N_3 \cos\left(\theta + \frac{\alpha}{2}\right) + P'_{c\,I} + P'_{c\,II} + P'_{c\,III}}{a_3 b_3} =$$

$$= \frac{2 \cdot \left(21094 + 2 \cdot 22207\right) \cdot 0.8036 + 4624 + 7592 + 9113}{0.0151 \cdot 0.028} = 299.5 \text{ MPa.}$$

9. Compare each calculated stress with the corresponding stress in the modern fir-tree roots (see para 4.3). Calculate safety factors for each stress. Mind that turbine blades operate at high temperatures. That is why long-term strength must be used as an admissible stress in this analysis.

The safety factors of each part must be calculated for each loading factor that generates the maximum stress:

– by the bearing stress, which arise at the contact surface of the i^{th} tooth of the root

$$k_{bear\ 2,3} = \frac{[\sigma_{0.2}]}{\sigma_{bear\ 2,3}} = \frac{700}{396.6} = 1.8;$$

– by the bending stress, which arise at the base of the ith tooth of the root

$$k_{bend\ 2,3} = \frac{[\sigma_{0.2}]}{\sigma_{bend\ 2,3}} = \frac{700}{249.7} = 2.8;$$

– by the shearing stress, which arise at the base of the ith tooth

$$k_{shear\ 1} = \frac{[\sigma_{0.2}]}{\sigma_{shear\ 1}} = \frac{700}{212.8} = 3.3;$$

– by the tensile stress at the neck of the ith tooth pair of the root

$$k_{tens\ I\ (2)} = \frac{[\sigma_{0.2}]}{\sigma_{tens\ I\ (2)}} = \frac{700}{249.6} = 2.8;$$

– by the tensile stress at the neck of the ith tooth pair of the steeple

$$k_{tens\ 3} = \frac{[\sigma_{0.2}]}{\sigma_{tens\ 3}} = \frac{700}{299.5} = 2.3.$$

The analysis of the results shows that all stresses (shearing, bearing and bending stress) arising in the designed joint of turbine blade and disk are approximately equal. Tensile stresses are the highest at the topmost neck of the blade root (the first tooth pair) and bottom neck of the disk steeple (the third tooth pair).

Shearing stress takes the pole position among all calculated stresses. The reason for this is the small width of contact surface of the tooth.

Norms of Strength are followed only for shearing stress that arises in the tooth. The stress state of the joint can be improved in the following ways. The first way concerns the acting load reduction or the change of the geometrical parameters of the joint in order to improve its securing capacity. This way can be implemented by the application of the shroudless blades. To preserve the efficiency drop, an engine must have the active clearance control system. The second way of improvement is the usage of a heat-resistant material or the optimization of the heat state of the joint.

REFERENCES

1. Филахтов, Ф. М. Расчет замков лопаток [Текст]: учеб. пособие / Ф. М. Филахтов. – Х.: ХАИ, 1972. – 39 с.

2. Скубачевский, Г. С. Авиационные газотурбинные двигатели. Конструкция и расчет деталей [Текст]: учеб. для вузов / Г. С. Скубачевский. – М.: Машиностроение, 1981. – 550 с.

3. Штода, А. В. Конструкция авиационных газотурбинных двигателей [Текст]: учеб. для вузов / А. В. Штода, В. А. Секистов, В. В. Кулешов; под общ. ред. А. В. Штоды. – К.: КВВАИУ, 1982. – 436 с.

4. Конструкция и проектирование авиационных газотурбинных двигателей [Текст]: учеб. для вузов / С. А. Вьюнов, Ю. И. Гусев, А. В. Карпов и др.; под общ. ред. Д. В. Хронина. – М.: Машиностроение, 1989. – 368 с.

5. Иноземцев, А. А. Основы конструирования авиационных двигателей и энергетических установок [Текст]: учебник / А. А. Иноземцев, М. А. Нихамкин, В. Л. Сандрацкий. – М.: Машиностроение, 2008. – Т.2. – 366 с.

6. ГОСТ 23537-79. Лопатки авиационных осевых компрессоров и турбин. Термины и определения. – Введ. 01.01.1980. – М.: Изд-во стандартов, 1979. – 30 с.

7. ОСТ 1 11031-81. Соединение лопаток с дисками типа «ласточкин хвост» ГТД. Конструкция и размеры. – Введ. 01.01.1988. – М.: Изд-во стандартов, 1981. – 16 с.

8. ОСТ 1 10780-72. Двигатели газотурбинные. Соединение лопаток с дисками типа «шарнир». Конструкция и размеры. – Введ. 01.07.1973. – М.: Изд-во стандартов, 1973. – 14 с.

9. ОСТ 1 10975-81. Соединения лопаток с дисками елочного типа газотурбинных двигателей. Конструкция и размеры. – Введ. 01.01.1983. – М.: Изд-во стандартов, 1981. – 93 с.

10. Писаренко, Г. С. Справочник по сопротивлению материалов [Текст] / Г. С. Писаренко, А. П. Яковлев, В. В. Матвеев. – К.: Наук. думка, 1988. – 736 с.

CONTENTS

Навчальне видання

Марценюк Євген Вікторович
Сіренко Фелікс Феліксович

РОЗРАХУНОК ЗАМКІВ РОБОЧИХ ЛОПАТОК

(Англійською мовою)

Редактор Н. Б. Зюбанова
Технічний редактор Л. О. Кузьменко

Зв. план, 2016
Підписано до друку 12.05.2016
Формат 60х84 1/16. Папір офс. № 2. Офс. друк
Ум. друк. арк. 2,8. Обл.-вид. арк. 3,25. Наклад 50 пр. Замовлення 154.
Ціна вільна

Видавець і виготовлювач
Національний аерокосмічний університет ім. М. Є. Жуковського
«Харківський авіаційний інститут»
61070, Харків-70, вул. Чкалова,17
http://www.khai.edu
Видавничий центр «ХАІ»
61070, Харків-70, вул. Чкалова, 17
izdat@khai.edu

Свідоцтво про внесення суб'єкта видавничої справи
до Державного реєстру видавців, виготовлювачів і розповсюджувачів
видавничої продукції сер. ДК № 391 від 30.03.2001